Nasal tissue-resident memory CD4$^+$ T cells persist after influenza A virus infection and provide heterosubtypic protection

Nimitha R. Mathew[1,*], Romain Gailleton[1], Lydia Scharf[1], Karin Schön[1], Josue Enriquez[1], Hannes Axelsson[1], Anneli Strömberg[1], Nils Lycke[1], Mats Bemark[1,2,3], Ka-Wei Tang[4,5], Davide Angeletti[1,6,*]

Running title: Nasal tissue CD4 TRM protect against influenza

Affiliations:

[1]Department of Microbiology and Immunology; Institute of Biomedicine; University of Gothenburg; Gothenburg; Sweden.

[2]Department of Clinical Immunology and Transfusion Medicine, Sahlgrenska University Hospital, Gothenburg, Sweden

[3]Department of Translational Medicine – Human Immunology, Lund University, Malmö, Sweden

[4]Department of Infectious Diseases, Institute of Biomedicine, University of Gothenburg, Gothenburg, Sweden

[5]Region Västra Götaland, Sahlgrenska University Hospital, Department of Clinical Microbiology, Gothenburg, Sweden

[6]SciLifeLab, Institute of Biomedicine; University of Gothenburg, Gothenburg, Sweden

*Corresponding authors. Email: nimitha.mathew@gu.se; davide.angeletti@gu.se

ABSTRACT:

CD4 tissue-resident memory T cells (TRM) are crucial adaptive immune components involved in preventing influenza A virus (IAV) infection. Despite their importance, their physiological role in the upper respiratory tract, the first site of contact with IAV, remains unclear. Here, we find that, after IAV infection, antigen-specific CD4 TRM persist in the nasal tissue (NT) compartment after infection and provide protection upon heterosubtypic challenge. Single cell RNA sequencing analysis reveals that NT CD4 TRM are heterogeneous and transcriptionally distinct as compared to their lung counterparts. Mechanistically, we demonstrate that the CXCR6-CXCL16 axis promotes CD4 TRM residency in the NT. Furthermore, we show that the NT of mice and humans contains a high frequency of Th17 CD4 TRM that aid in local viral clearance and in reducing tissue damage. Collectively, our results support a robust physiological role for nasal tissue CD4 TRM in local protection during heterosubtypic IAV infection.

INTRODUCTION

Influenza A virus (IAV) continues to pose a threat to society by causing yearly morbidity, deaths and providing a fertile ground for opportunistic bacterial infections (Paget et al., 2019). Seasonal vaccines elicit antibodies against the immunodominant surface glycoprotein hemagglutinin (HA) which is, however, prone to antigenic drift. Therefore, vaccines show limited effectiveness and are updated annually (Campbell et al., 2020). In addition, there is a hovering risk of pandemics caused by the recombination of animal and human viruses (The, 2024). Under such circumstances, antibody-mediated protection is usually inefficient. However, memory T cells recognize IAV internal proteins which are relatively conserved across different strains (Vijayanand et al., 2020), thus mediating heterosubtypic responses.

Among the memory T cells, tissue resident memory T cells (TRM) are gaining traction as a 'ready to deploy' memory arm that is formed at the site of infection and hence acts as a barricade before the pathogens reach the circulation or lymphoid organs where effector memory or central memory T cells can be activated (Marchesini Tovar et al., 2024). Indeed, during IAV infection, both CD4 and CD8 TRM in the lungs protect against heterologous viruses (Teijaro et al., 2011; Zheng et al., 2023). Compared to CD8 TRM, CD4 TRM are understudied, despite their multifunctionality. They can mediate viral clearance, act by direct cytotoxicity on virus-infected

55 cells, guide the formation of IAV-specific lung CD8 TRM and orchestrate local B cell responses
56 (Borkner et al., 2021; Brown et al., 2012; Son et al., 2021; Swarnalekha et al., 2021; Teijaro et
57 al., 2011). Specifically, lung CD4 TRM are diverse and exhibit different functions depending
58 on their antigenic specificity. For example, two subsets of IAV NP (nucleoprotein)- specific
59 lung CD4 TRM were recently identified: $T_{RM}1$ which are Th1 like, and T follicular helper like
60 cells (T_{RH}) which are involved in promoting local antibody response and delivering help to local
61 CD8 T cells (Son et al., 2021; Swarnalekha et al., 2021). On the other hand, M2e (ectodomain
62 of virus matrix protein)-specific lung CD4 TRM were shown to be mostly of the Th17 subtype
63 and protect from tissue injury during IAV infection (Omokanye et al., 2022). However, our
64 knowledge about CD4 TRM in other tissues relevant for respiratory viral infection is still
65 limited.

66 The upper respiratory tract (URT) is the port of entry for any inhaled pathogen and the first site
67 of contact with the immune cells of the body. The immune system within the mouse URT is a
68 complex network of draining cervical lymph nodes (cLN), nasal-associated lymphoid tissues
69 (NALT) and immune cells dispersed within the nasal chamber outside the NALT (referred as
70 nasal tissues; NT) (Pizzolla et al., 2017a; Randall). The NALT is the site for the recall expansion
71 of memory T cells and priming of naïve T cells, whereas cLN act as a priming site (Liu et al.,
72 2024; Pizzolla et al., 2017b). Increasing evidence suggest that protective CD4 TRM are
73 generated during bacterial and SARS-CoV-2 infection in the URT (Borkner et al., 2021; Diallo
74 et al., 2023a; Kinnear et al., 2018; Lim et al., 2022; O'Hara et al., 2020; Wimmers et al., 2023;
75 Xu et al., 2023; Yount et al., 2023). Nevertheless, the cues needed for URT CD4 TRM formation
76 and tissue residency remain elusive. For IAV, some studies have demonstrated the protective
77 role of URT CD8 TRM in reducing viral burden and transmission (Pizzolla et al., 2017a;
78 Richard et al., 2020; Uddbäck et al., 2024). Surprisingly, despite the importance of CD4 TRM
79 and the extensive spread of IAV, the role of IAV-specific CD4 TRM in URT has not been
80 explored.

81 Here, we investigate antigen-specific CD4 TRM within the URT of IAV-infected mice and
82 healthy human volunteers. We demonstrate that CD4 TRM form in NT of the URT and protect
83 upon a heterologous IAV infection. Furthermore, we discover transcriptional differences
84 between TRM populations in NT *vs* lungs and define factors required for the formation of

85 antigen-specific CD4 TRM in the NT. Our data provide a comprehensive characterization of
86 previously unexplored, IAV-specific CD4 TRM cells that reside in the URT.

87

88 **RESULTS**

89 ***IAV infection generates long-lived antigen specific CD4 TRM in the nasal tissue***

90 To assess whether IAV-specific CD4 TRM arise in the URT, splenic CD4 T cells derived from
91 Ovalbumin (OVA)-specific OT-II T cell receptor (TCR) transgenic mice that could be identified
92 as CD45.1^{+} or tdTomato^{+} were transferred into congenic C57BL/6J (CD45.2^{+}) mice.
93 Subsequently, we infected the mice intranasally (i.n.) with a mouse-adapted IAV strain PR8
94 H1N1 that expresses the $OVA_{323-339}$ peptide (PR8-OVA) and examined NALT and NT for
95 OVA-specific CD4 TRM (OT-II CD4 TRM) on day 30 post infection. We used lungs as a
96 positive control because IAV specific CD4 TRM are well known to form there (Teijaro et al.,
97 2011). Throughout all our experiments, we administered fluorochrome-conjugated CD4
98 antibody intravenously (i.v.) 5 minutes before sacrifice to distinguish CD4 T cells in the tissue
99 from those in the vasculature (Fig 1A). CD4 memory T cells were identified as being CD3^{+},
100 CD4^{+}, CD44^{+} and CD62L^{-}. We differentiated CD4 TRM from their circulating counterparts as
101 CD3^{+}CD4^{+}CD44^{+}CD62L^{-} i.v.$^{-}$ CD69^{+} (Fig S1A). CD69 is a well-known tissue retention
102 molecule that prevents egress of T cells from the tissue(Shiow et al., 2006; Szabo et al., 2019b).
103 OT-II CD4 TRM were present in the NT at a similar frequency as lungs. However, we found
104 less OT-II CD4 TRM in the NALT (Fig 1B-C).

105 To localize OT-II CD4 T cells anatomically within the URT, we isolated, fixed and decalcified
106 heads of PR8-OVA infected mice on day 30 post infection. OT-II CD4 T cells were found
107 throughout the nasal chamber, including the olfactory epithelium (OE), respiratory epithelium
108 lining the nasal septum (S), maxilloturbinates (MT) and NALT (Fig 1D). Given the localization
109 of OT-II CD4 T cells in proximity to the epithelium of the NT, we examined the expression of
110 CD103, an integrin involved in the adhesion of T cells to E-cadherin on epithelial cells. CD103
111 is often associated with CD8 TRM (Beura et al., 2019; Szabo et al., 2019b; Zens et al., 2017)
112 but its association with CD4 TRM in the respiratory tract has not been elucidated, in mice.
113 Indeed, CD103 was poorly expressed on lung CD4 TRM in comparison to NT CD4 TRM (5%
114 *vs* 22%) (Fig 1E-F, Fig S1B). Apart from CD103, we analyzed NT CD4 TRM for the expression
115 of CD11a, another marker associated with TRM residency at late days after infection (Szabo et

al., 2019b; Teijaro et al., 2011). Nearly all OT-II CD4 TRM in the NT and lungs expressed CD11a (Fig 1E-F, Fig S1B).

Having demonstrated that NT CD4 TRM are established in a transfer model, we wanted to verify whether they would also form when precursor frequency is at physiological levels. Hence, we took advantage of MHC-II tetramers, presenting immunodominant peptides I-A^b HA_{91-107} and I-A^b $NP_{306-322}$ (Besavilla et al., 2023; Miller et al., 2015). To follow the kinetics of antigen specific CD4 TRM, we infected mice with PR8 and harvested the lungs and NT at different time points (Fig 1G). We found that I-A^b HA_{91-107} tetramer$^+$ and I-A^b $NP_{306-322}$ tetramer$^+$ CD4 TRM arose as early as 10 day post infection (dpi). The number of tetramer$^+$ CD4 TRM declined from day 10 to day 30. Although, there was a steady decrease in tetramer-specific CD4 TRM in NT and lungs, we could still detect antigen-specific CD4 TRM in the NT on 120 dpi in most of the mice, suggesting this to be a relatively stable population (Fig. 1H-I, Fig S1C-E). We observed similar long-term kinetics for OT-II$^+$ CD4 TRM in the OT-II transfer model (Fig 1I, Fig S1C-D).

IAV-specific CD4 TRM in the lungs are self-sustaining, without being replenished from the lymphoid reservoirs(Turner et al., 2014). To determine whether the same was true for NT CD4 TRM, we analyzed their expression of Ki-67, a marker for ongoing cell division (Miller et al., 2018). As expected, at the early stage after infection (10 dpi) approximately 60% of the IAV-specific NT CD4 TRM expressed Ki-67 (Fig 1J, Fig S1F), suggesting that some of those may still be in the effector phase. Conversely, at early (30 dpi) and late (60 dpi) memory time points only 10-15% of I-A^b HA_{91-107} tetramer$^+$ and I-A^b $NP_{306-322}$ tetramer$^+$ NT CD4 TRM expressed Ki-67, indicating a low level of homeostatic proliferation (Fig 1J, Fig S1F). The importance of cognate antigen for the formation of TRM varies depending on tissue and T cell type; cognate recognition is a crucial factor for lung CD8 TRM formation(Takamura et al., 2016) but it is not required by NT CD8 TRM(Pizzolla et al., 2017a). Thus, we sought to assess the importance of cognate antigen maintenance for NT CD4 TRM formation. We generated effector tdTomato$^+$ OT-II T cells *in vitro* and transferred them to C57BL/6 mice that were infected with either PR8 or PR8-OVA two days prior (Pizzolla et al., 2017a) (Fig 1K). In this model, even though effector OT-II cells can access the NT in both PR8 and PR8-OVA infected groups, we found that OT-II CD4 TRM were only retained in the NT of the PR8-OVA-infected mice (Fig 1L-M). This was also observed for lung CD4 TRM (Fig S1G-H). Our results demonstrate that cognate antigen,

147 rather than only an inflammatory milieu, is required for the conversion of effector OT-II T cells
148 to OT-II CD4 TRM in respiratory mucosal tissues, in contrast to NT CD8 TRM (Pizzolla et al.,
149 2017a).

150 In summary, we found that IAV-specific CD4 TRM are generated and persist in the NT
151 following infection.

152 ***NT CD4 TRM are multifunctional and produce cytokines upon antigen stimulation***

153 A rapid and efficient response to viral re-infection is a key feature of memory T cells, including
154 CD4 TRM. Upon recognition of their specific antigen, memory T cells are reactivated and
155 produce cytokines, some of which have a direct impact on virus-infected cells while others
156 influence the recruitment of additional immune cells(Künzli and Masopust, 2023). To evaluate
157 the IAV-specific response in NT CD4 TRM, we stimulated NT and lung cells including CD4
158 TRM from PR8-infected mice with an IAV-derived nucleoprotein (NP) peptide pool. Compared
159 to unstimulated controls or naïve NT CD4 TRM, a higher proportion of peptide-stimulated NT
160 CD4 TRM produced IFN-γ and IL-2, while no change was observed for TNF (Fig 2A-B and
161 Fig S2A). Similarly, CD4 TRM sorted from either NT or lungs expressed higher amounts of
162 intracellular IFN-γ when stimulated with splenocytes pulsed with NP peptide pool compared to
163 SARS-CoV-2 nucleocapsid peptide pool, ruling out a role for ongoing inflammation in IFN-γ
164 production (Fig 2C-D). NT and lung CD4 TRM displayed a similar immunodominance profile
165 with regards to different IAV-derived peptides stimulation (Fig S2B). In general NT CD4 TRM
166 harbored a lower frequency of cytokine producing cells than lung CD4 TRM (Fig 2A-D, Fig
167 S2A). To exclude the possibility that this was due to that NT CD4 TRM had a more exhausted
168 phenotype we measured PD-1 expression. CD4 TRM from both organs had a similar frequency
169 of PD-1^{+} CD4 TRM indicating this was not the case (Fig 2E-F, Fig S2C) but suggesting a role
170 for PD-L1-PD1 axis in CD4 TRM regulation, similarly to what was described for IAV-specific
171 CD8 TRM(Wang et al., 2019). Surprisingly, even though NT CD4 TRM had overall lower
172 frequency of cytokine producing cells, ICOS, a T cell co-stimulatory molecule (Moguche et al.,
173 2015; Peng et al., 2022), was expressed on a higher proportion of NT CD4 TRM in comparison
174 to lung CD4 TRM (Fig 2E-F, Fig S2C).

175 ***NT CD4 TRM provide protection upon heterologous IAV challenge***

176 CD4 TRM promote viral clearance by recruiting and activating B cells, CD8 T cells and innate
177 cells and by exerting direct cytotoxic effects on virus-infected cells(Künzli and Masopust,
178 2023). Given that NT CD4 TRM displayed an IAV-specific response (Fig 2A-D, Fig S2A), we
179 set out to elucidate their function upon heterosubtypic challenge. To test this, we infected mice
180 with PR8 and challenged them with heterologous X31 H3N2 virus on day 30 post primary
181 infection. X31 has identical internal proteins to PR8 (including NP) but distinct surface
182 glycoproteins (e.g. HA). First, we verified whether CD4 TRM respond to and expand locally at
183 6 days post rechallenge (Fig 3A). To rule out any contribution of circulating lymphocytes, we
184 treated the mice with FTY720 during the experiment (Brinkmann et al., 2002). Indeed,
185 frequencies of I-A^b $NP_{306-322}$ $tetramer^+$, but not I-A^b HA_{91-107} $tetramer^+$, CD4 TRM sharply
186 increased in both NT and lungs (Fig 3B-C and Fig S3A). The increase in I-A^b $NP_{306-322}$ $tetramer^+$
187 CD4 TRM was not due to expansion of naïve cells as it was not observed upon primary X31
188 infection (Fig S3B).

189 To define a possible role in protection, we performed the same experiment as above but instead
190 measured the viral titer in NT on day 3 post X31 infection. In addition to FTY720 treatment,
191 we depleted either CD4 T cells, CD8 T cells or both (Fig 3D). To effectively clear TRM from
192 respiratory mucosal tissues we injected mice with a high dose of depleting mAbs (Goplen et al.,
193 2020; Son et al., 2021) (Fig 3E and Fig S3C-D). In the absence of any intervention, the
194 secondary infection was cleared from the NT by cross-reactive T cells (Fig 3F), as PR8-
195 antibodies did not neutralize X31 (Fig S3E). Surprisingly, depletion of CD8 T cells did not
196 affect the viral clearance in the NT (with or without FTY720 administration) bolstering the role
197 of CD4 TRM in local protection. Conversely, CD4 T cell depletion severely impaired viral
198 clearance, with viral titers similar to those of the mice that did not undergo a primary infection
199 (Fig 3F). To further exclude any possible contribution of lung TRM, despite FTY720
200 administration, we used an intratracheal infection (i.t.) model for the primary IAV inoculation
201 (Fig 3G). Upon i.t. infection, IAV-specific CD4 TRM formed only in the lungs but not in the
202 NT (Fig S3F). Accordingly, heterologous i.n. X31 challenge, combined with FTY720,
203 administration resulted in the expansion of I-A^b $NP_{306-322}$ $tetramer^+$ CD4 T cells only in lungs
204 but not in NT (Fig 3H-I). When compared to local expansion after i.n. prime (Fig 3B), the results
205 strongly suggest that TRM are the major players involved in the local response. In addition, we
206 repeated the CD4 depletion experiment (Fig 3G) combined with i.n. or i.t. prime and X31

207 challenge (Fig 3J): as expected, CD4 depletion affected viral titers in lungs. Conversely, i.n.
208 primed mice (both NT and lung CD4 TRM) had lower viral titers in NT when compared to i.t.
209 primed mice (only lung TRM) and CD4 treatment impaired protection in NT only when local
210 CD4 TRM were present (Fig 3J). Our overall results (Fig 3F-J) strongly support that NT CD4
211 TRM contribute to protection independently of lung CD4 TRM.

212 To verify whether NT CD4 TRM were also induced by vaccination, we established an i.n.
213 vaccination model using CTA1-3M2e-DD as an immunogen. CTA1-3M2e-DD contains 3
214 tandem repeats of M2e linked to CTA1-DD adjuvant; M2e is highly conserved across IAVs and
215 immunization with CTA1-3M2e-DD has been shown to induce M2e specific lung resident CD4
216 T cells that protect against lethal IAV challenge in mice(Eliasson et al., 2008; Eliasson et al.,
217 2018). For these experiments, we used BALB/c rather than C57BL/6 as CTA1-3M2e-DD
218 induces poorer M2e specific T cell responses in C57BL/6(Eliasson et al., 2018). To maximize
219 the formation of CD4 TRM in NT and not lung, we modified the immunization protocol and
220 reduced the volume to 5µl. We vaccinated mice with three i.n. doses of CTA1-3M2e-DD or
221 CTA1-DD and evaluated the M2e specific CD4 Tc response on day 30 (day 10 after last
222 vaccination) (Fig S3G). Like the response observed after infection, we found that I-A^d $M2e_{2-17}$
223 tetramer$^+$ CD4 Tc robustly formed in the NT (Fig S3H-I). Furthermore, I-A^d $M2e_{2-17}$ tetramer$^+$
224 CD4 TRM formed and persisted only in the NT and cLN on day 50 (day 30 after last
225 vaccination) with almost none in the lungs and few in mediastinal lymph nodes (MLN) (Fig
226 S3J-M). To ascribe a role to M2e-specific CD4 TRM, we immunized mice with CTA1-DD or
227 CTA1-3M2e-DD and challenged them at day 50 with high dose of PR8 in low inoculum
228 volume, to restrict initial viral replication to the URT (Gailleton et al., 2025) (Fig S3N). This
229 immunization strategy mainly generates M2e-specific CD4 TRM with no CD8 TRM (Eliasson
230 et al., 2018). After challenge, 45% of the mice that were immunized with the control succumbed
231 to the disease, however, immunization with CTA1-3M2e-DD protected against mortality and
232 reduced weight loss (Fig S3O-P). Surprisingly, we could not detect differences in viral titers in
233 neither lungs nor NT between the groups suggesting that M2e-specific CD4 TRM rely on other
234 mechanisms for protection than viral control (Fig S3Q), as previously observed (Omokanye et
235 al., 2022).
236 Taken together, our findings revealed that NT CD4 TRM are important for protection during
237 heterosubtypic infection.

238 ***CD4 TRM in the lungs and NT are heterogeneous, but Th17 cells are prevalent in the NT.***

239 Having identified the dynamics and role of NT CD4 TRM, we wanted to investigate the
240 transcriptional differences between total and antigen-specific CD4 TRM in NT *vs* lungs.
241 Therefore, we performed scRNA-seq together with scTCR-seq at 30 dpi. Mice were injected
242 with CD4 antibody i.v. 5 minutes before sacrifice and total CD4 TRM, I-A^b HA_{91-107} $tetramer^+$
243 and I-A^b $NP_{306-322}$ $tetramer^+$ CD4 TRM were sorted from NT and lungs of mice (Fig. 4A).
244 Furthermore, we also sequenced a small proportion of all live cells, which were $CD4^-$. To
245 maximize the number of cells and samples that could be loaded simultaneously, different
246 samples were labeled with hashtag antibodies. Data from all mice and organs were integrated,
247 processed, and visualized on a two-dimensional UMAP (Fig 4B). T cell subpopulations were
248 assigned based on well-known markers and gene signatures (Fig 4C, Fig S4A-B and Table S1).
249 The major T cell subpopulation was, as expected given the intracellular viral infection, Th1
250 cells (Fig S4C) defined by a well-established signature(Andreatta et al., 2022), including *Ifng*
251 and *Cxcr3*. Cytotoxic CD4 T cells were present in both organs and defined by *Nkg7*, *Fasl*, *Ccl4*,
252 *Ccl5* and a CD4 cytotoxic signature(Hashimoto et al., 2019). We were unable to properly define
253 a third major cluster, C.3; this cluster harbored several mitochondrial genes, even though all
254 mitochondrial genes were regressed out and did not contribute to the clustering. Therefore, we
255 believe these cells to be either senescent/dying cells or highly proliferative cells. Tfh cells were
256 generally more prevalent within lungs (Fig S4C), consistent with a possible role in supporting
257 ectopic GC in iBALTs. Based on their transcriptional profile they were separated into two
258 clusters, named Tfh.1 and Tfh.2. Tfh.1 were Tfh cells with strong expression of *Tnfsf8*, *Bcl6*,
259 and a signature previously associated with Tfh (Andreatta et al., 2022). Nevertheless, Tfh.2 had
260 higher expression of other Tfh-associated genes such as *Tox*, *Slamf6* and *Pdcd1*. C.5 cells
261 expressed several transcription factors, *Cd40lg* but also had high expression of genes involved
262 in regulation of NF-kB signaling (*Nfkbia*, *Nfkbid*, *Nfkbiz*). This cluster has been previously
263 reported and suggested to include cells which are poised to rapidly respond to secondary
264 infections by producing cytokines (Kurd et al., 2020; Woodring et al., 2022). Quiescent memory
265 cells were slightly more prevalent within NT and characterized by the expression of several
266 long non-coding RNAs (including *Malat1*)(Dey et al., 2023; Plasek and Valadkhan, 2021) and
267 low ribosomal gene expression. A small proportion of our CD4 TRM was naïve-like T cells
268 expressing *Ccr7*, *Sell* and *Klf2 (Wang et al., 2022)*. Furthermore, we identified Tregs by *Foxp3*

269 expression and Treg-signature(Yang et al., 2021). Early activated cells were defined based on
270 the expression of genes linked with migration within the tissue, such as *Gpr183(Li et al., 2016)*,
271 and signaling receptors such as *Ms4a4b*(Yan et al., 2012) suggesting an overall movement
272 within the tissue but also modulation of T cell activation. NKT cells and IFN responsive cells
273 were clearly identified by their distinctive signatures: the former expressed *Klrd1*, *Klrk1*,
274 *Klrb1c*(Cohen et al., 2013; Hu et al., 2022) and other cytotoxic genes (*Nkg7*, *Fasl*)(Ng et al.,
275 2024; Tuomela et al., 2022) while the latter was enriched for Interferon stimulated genes (*Isg15*,
276 *Ifit3*, *Ifit1*), a signature similar to one previously identified in human CD4(Szabo et al., 2019a).
277 Strikingly, Th17 cells, expressing *Rorgc*, *Il17a*, *Tmem176a* and *Ccr6* were much more abundant
278 within NT(Szabo et al., 2019a) (Fig S4C and Table S1). We were also able to identify several
279 endothelial and epithelial airway cells clusters, from the live cell fraction devoid of CD4 T cells.

280 Overall, our scRNASeq analysis highlighted the diversity and variety of CD4 TRM
281 subpopulations in both lungs and NT. While Th1 and cytotoxic CD4 T cells made up almost
282 50% of the total TRM in both lungs and NT, consistent with an intracellular viral infection, their
283 relative proportions were similar between organs (Fig. S4C). Interestingly, IAV infection did
284 not appear to majorly reshape the CD4 TRM landscape in terms of the abundance of cell type
285 (Fig S4D). Therefore, to confirm our results and limit our analysis to influenza-specific cells,
286 we subsetted the CD4 cells to only include the tetramer$^+$ cells. Indeed, this did not change the
287 proportion of CD4 TRM, confirming an increased abundance of both HA$^+$ and NP$^+$ Th17 cells
288 within the NT, while these cells were almost absent in lungs (Fig 4D and Fig S4E). By
289 visualizing the distribution of HA$^+$ and NP$^+$ cells as density plots we established that antigen-
290 specific cells differentiated into almost all CD4 TRM subsets, except for Th17 in the lungs.
291 However, the density distribution in NT was dramatically different between the two proteins,
292 with NP$^+$ cells being mostly Th17 and Th1 while HA$^+$ cells also included many cytotoxic and
293 Tfh CD4 TRM cells (Fig 4D and Fig S4E).

294 ***CD4 TRM within the NT exhibit a distinct transcriptional profile, compared to lungs.***

295 The power of the single cell approach is that it allows transcriptional differences to be compared
296 between the same CD4 TRM subtypes, depending on the organ. Therefore, we performed
297 differential gene expression (DEG) analysis for each cell subpopulation and visualized the
298 results with both heatmap and volcano plots (Fig S4F-G and Table S1). As expected, the

299 majority of CD4 TRM subpopulations exhibited similar gene expression between organs,
300 however Th1, Cytotoxic CD4, Tfh.1 and Th17 clusters were the ones with most organ-specific
301 differences. For Th1, lung cells had higher expression of *Ccr2*, a chemokine receptor previously
302 linked with pulmonary homing(Brownlie et al., 2022; Hoft et al., 2019), *Ctla4* but also *Ifng* and
303 *Nfkbia,* suggesting a more active and productive phenotype, compared to that of their NT
304 counterpart, in line with what we observed above (Fig 2A-B). On the other hand, NT Th1 were
305 enriched for other essential transcription factors such as *Crem* and *Taf7* which are involved in
306 cytokine production(Devaiah et al., 2010; Rauen et al., 2013) and *Xcl1*, which promotes Treg
307 differentiation(Nguyen et al., 2008), suggesting an overall more immune-suppressive state.
308 Cytotoxic CD4 cells had similar pattern with *Ccr2* and genes associated with a more active
309 phenotype expressed in the lungs. Interestingly, NT CD4 TRM upregulated several chemokine
310 receptors, including *Cxcr6* and *Ccr8,* and many other factors previously associated with T cells
311 at mucosal sites (such as *Spp1* and *Penk*)(Kourepini et al., 2014; Mas-Orea et al., 2023).
312 Remarkably, *Cxcr6* was also significantly upregulated in NT Tfh.1 and Th17 clusters. In
313 addition, Tfh.1 NT cells also shared *Tff1* and *Xcl1* upregulation with other clusters, while NT
314 Th17 exhibited increased *Crem* and *Nr4a2* expression.

315 In summary, several CD4 TRM subpopulations displayed differential gene expression between
316 lungs and NT, with the lung cells showing a more activated phenotype and higher *Ccr2*
317 expression, consistent with their localization. Conversely NT CD4 TRM expressed genes
318 commonly associated with T cells at mucosal sites and with an immune-dampening phenotype,
319 with several clusters also expressing the chemokine receptor *Cxcr6*.

320 ***Expanded clonotypes have multiple fates and populate both lungs and NT.***

321 Having identified differences between CD4 TRM residing in different organs we wanted to
322 investigate whether T cell clones were compartmentalized or shared between them. A caveat of
323 our experimental procedure is that we had to pool several mice to obtain sufficient numbers of
324 antigen-specific cells and, therefore, we were not able to define clonality at the single mouse
325 level. However, a previous study suggested that $CD4^+$ T cell responses are largely private even
326 for a single viral-peptide specificity(Andreatta et al., 2022). Consistent with the notion of a
327 largely private response we did not detect any exaggeratedly expanded T cell clones, with only
328 5 families with more than 30 members. Expanded clones were distributed across the majority

329 of CD4 TRM subpopulations within the lungs, except for the naïve, Treg, NKT and Th17 which
330 were composed mainly of single clones (Fig 4E). Conversely, NT exhibited a higher clonal
331 expansion within Th17. When focusing only on antigen-specific clones, we detected a very
332 similar pattern of clonal expansion (Fig S5A). To visualize the specificity, organ and
333 subpopulation distributions, we plotted the top 34 expanded clones (Fig 4F). This confirmed the
334 pattern of expansion and that most of expanded clones were shared among several
335 subpopulations but also between organs. Validating our tetramer sorting approach, clones were
336 either HA or NP specific, however, in many cases, we did not sort all clones within the same
337 family, as also expected. Substantiating the private nature of TCR responses was the fact that
338 many of the NP expanded clones had similar, but not identical, CDR3 sequences (Fig 4F). This
339 suggests that certain TCRs had higher affinity for NP peptide but stochastic variations, not
340 altering binding, were present in different mice. Indeed, analysis of paired TCRa-TCRb usage
341 demonstrated a strong bias in NP responses for TRAV6-7_TRBV3 for both lungs and NT (Fig
342 S5B). By visualizing with a bubble plot, in which the size of the bubble is proportional to the
343 clone size, we revealed that many of the more expanded, antigen-specific clones in the lungs
344 were also shared with the NT (Fig 4G). This points toward a common origin within the same
345 lymph nodes and subsequent migration to tissues of residency. Finally, to determine whether
346 certain clonotypes were more prone to direct CD4 TRM toward a certain fate we utilized the
347 "clonotype bias" measure introduced by Andreatta et al.(Andreatta et al., 2022) and
348 implemented within the scRepertoire package(Borcherding et al., 2020). The analysis revealed
349 that the majority of clonotypes were largely unbiased with few exceptions (Fig S5C).
350 Interestingly, clonotype bias strongly correlated with being organ-specific (Fig S5C-D). For
351 instance, the third largest clone was present only in the lungs and over 60% of its members
352 belonged to the Tfh.2 cluster (Fig S5C-D). Likewise, the only large clone found exclusively in
353 NT had just shy of 50% of its members belonging to the early activated CD4 TRM group (Fig
354 S5D). However, the most expanded clones were generally not biased, despite having a strong
355 prevalence of Th1 and Tfh.1 cells (Fig S5E). The tendency of the few biased clones to be organ
356 specific could also suggest local proliferation and expansion.

357 Combined TCR analyses unveiled how most CD4 TRM clonotypes can differentiate into
358 multiple fates and then reside in both lungs and NT. However, there were few clones that were
359 tissue-specific, and they tended to be biased toward one CD4 T cell subtype.

360 ***CXCR6-CXCL16 axis promotes CD4 TRM recruitment to the NT***

361 Given that *Cxcr6* was highly expressed in several NT clusters (Fig S4F-G) we further explored
362 the mechanistic involvement of this chemokine receptor in the migration of effector CD4 T cells
363 to the NT. First, we confirmed *Cxcr6* to be the most interesting candidate as it was more highly
364 expressed in NT CD4 TRM than in lung CD4 TRM (Fig 5A-C). In particular, the clusters of
365 cytotoxic CD4 T cells, Tfh.1, Th17, Treg, early activated and Tfh.2 displayed higher expression
366 of *Cxcr6* in NT (Fig 5B). CXCR6 is known to be predominantly expressed in CD8 TRM rather
367 than circulating CD8 T cells (Mabrouk et al., 2022). Similarly, we found high CXCR6
368 expression in CD4 TRM and low expression in CD4 effector memory T cells (TEM i.v.$^{+}$) of
369 IAV-infected mice (Fig 5D). While CXCR6 expression was greater in infected NT than lungs,
370 its expression was similar to that of NT CD4 TRM in naïve mice (Fig 5D). This may seem
371 surprising, however, by definition, TRM are not naïve cells and therefore their presence in NT
372 has been triggered by a previous insult. Furthermore, we also found higher CXCR6 expression
373 among antigen specific OT-II TRM in NT *vs* lungs (Fig 5E-F).

374 Within the lungs, CXCR6 is essential for the positioning of CD8 TRM in the airways but not in
375 the lung interstitium after IAV infection(Wein et al., 2019). To determine whether CXCR6 is
376 required for the establishment of CD4 TRM in the NT, we generated WT-*Cxcr6*$^{-/-}$ bone marrow
377 (BM) chimeras. To do this, we lethally irradiated congenic C57BL/6 (CD45.1^{+}) (recipient) to
378 deplete the host bone marrow and reconstituted them with equal numbers of tdTomato^{+} WT BM
379 (CD45.2^{+}) and tdTomato^{-} *Cxcr6*$^{-/-}$ BM (CD45.2^{+}) (Fig 5G). Blood chimerism was verified on
380 day 67 post BM transfer, with almost 90% of the leukocytes being donor-derived. Interestingly,
381 we detected a higher frequency of *Cxcr6*$^{-/-}$ leukocytes in the blood (Fig S6A). On day 70 post
382 BM transfer, we infected the mice and analyzed organs at day 30 post infection. CXCR6
383 expression helped in lodging total and I-A^{b} NP$_{306-322}$ tetramer^{+} CD4 TRM in both NT and lungs,
384 as we observed a reduced frequency of *Cxcr6*$^{-/-}$ CD4 TRM in comparison to WT CD4 TRM in
385 both compartments (Fig 5H-J). Surprisingly, we found that 6 out of 13 chimeric mice had too
386 few I-A^{b} NP$_{306-322}$ tetramer^{+} CD4 TRM in the NT for downstream analysis, from both WT and
387 KO cells (Fig 5J). We speculate that this may be due to a generally low level of donor T cell
388 chimerism achieved at the NT in comparison to that in the lungs (Fig S6B). The finding that NT
389 CD4 TRM are not easily depleted or replenished, consolidate our data about longevity of these
390 cells, i.e. that once they are formed and reside in the NT they will persist. Moreover, we detected

391 an increased accumulation of *Cxcr6*$^{-/-}$ CD4 T cells in the blood, spleen, lung-draining
392 mediastinal lymph nodes (mLN) and URT-draining cervical lymph nodes (cLN), confirming
393 the hypothesis that *Cxcr6*$^{-/-}$ CD4 T cells have migratory defects and/or they are not retained at
394 the tissue (Fig 5K).

395 CXCL16 is the only known ligand for CXCR6. It exists in both transmembrane and soluble
396 forms and acts as an adhesion molecule and a chemoattractant for leukocytes(Koenen et al.,
397 2017; Wilbanks et al., 2001). In murine lungs, CXCL16 colocalizes with Epcam and its
398 expression is restricted to the large airways lining the lungs(Wein et al., 2019). We investigated
399 CXCL16 expression in NT by microscopy and demonstrated that CXCL16 is expressed in the
400 NT of PR8-OVA infected mice and some OT-II CD4 TRM localize near CXCL16 (Fig 5L, Fig
401 S6C). Finally, to examine the contribution of CXCL16 to the early recruitment of effector CD4
402 T cells to the NT and lungs, we treated PR8-infected mice with α-CXCL16 antibody (Fig 5M).
403 α-CXCL16 treatment significantly reduced the frequency and number of I-A^{b} NP$_{306-322}$
404 tetramer^{+} CD4 TRM retained in the NT and, to a lesser extent, in the lungs (Fig 5N-O).

405 Altogether, we showed that CXCL16 production by airway cells and CXCR6 expression on
406 CD4 T cells are promoting the recruitment of CD4 effector memory T cells to respiratory
407 mucosal tissues and the subsequent establishment of TRM.

408 ***Healthy humans harbor IAV-responsive CD4 TRM in the nasal mucosa.***

409 Given the importance of IAV-specific CD4 TRM in the NT of mice, we wanted to investigate
410 whether a similar population exists in healthy human adults. As every individual is exposed to
411 IAV by the age of three(Bodewes et al., 2011), healthy adults must have undergone several
412 symptomatic and asymptomatic infections, and we hypothesized that they should maintain IAV-
413 specific CD4 TRM in their NT. The recruited subjects did not have any respiratory infection or
414 symptoms in the two weeks prior to the study, to avoid contamination from recently activated
415 CD4 T cells. We collected nasopharyngeal swab (NT) and peripheral blood mononuclear cells
416 (PBMC) and analyzed T cells by flow cytometry (Thome et al., 2014) (Fig S7A-B). While the
417 frequency of naïve CD4 T cells (CD3^{+}CD4^{+}CD45RA^{+}CCR7^{+}) was higher in PBMCs, CD4
418 central memory T cells (TCM) (CD3^{+}CD4^{+}CD45RA^{-}CCR7^{+}) and CD4 terminally
419 differentiated effector memory T cells re-expressing CD45RA (TEMRA) did not show any
420 difference (Fig S7C). Interestingly, CD4 TEM (CD3^{+}CD4^{+}CD45RA^{-}CCR7^{-}) were higher in NT

421 with their subpopulation TRM ($CD3^+CD4^+CD45RA^-CCR7^-$ $CD69^+$) being exclusively present
422 in NT of all subjects, albeit in varying numbers. When we analyzed both PBMCs and NT, we
423 found that NT CD4 TRM included CD103 (18%) and CXCR6 expressing cells (23%) as
424 previously reported(Ramirez et al., 2024) while PBMC CD4 TEM barely expressed them,
425 similar to our findings in mice (Fig 6A-B).

426 A longitudinal study on SARS-CoV-2 vaccinees who had breakthrough infections showed
427 functional NT T cells, specific for SARS-CoV-2 proteins, that persisted for ≥140 days(Lim et
428 al., 2022). Given the relatively long lifespan of NT CD4 T cells, we wanted to examine whether
429 healthy adults retained IAV-specific NT CD4 TRM, acquired by encountering IAV at some
430 timepoint in life. To do that, we stimulated PBMC and NT cells with IAV peptide pools derived
431 from the internal proteins NP and M1 (Matix protein 1) and assessed cytokine expression. We
432 found that PBMC CD4 TEM from 79.5% of the subjects responded to stimulation by secretion
433 of IFN-γ (Fig 6C). Conversely, we did not detect an IFN-γ response in NT CD4 TRM after
434 stimulation. Furthermore, we found no detectable TNF response from NT or PBMCs CD4 T
435 cells (Fig 6C). As the scRNA-seq mouse experiment had revealed high frequencies of Th17
436 cells in NT (Fig 4E), we also tested if IL-17a expression was induced in stimulated cells.
437 Intriguingly, in NT CD4 TRM the frequency of IL-17a expressing cells increased after
438 stimulation in 63.2% of the individuals. Little to no IL-17a expression was detected in PBMCs
439 before or after stimulation (Fig 6C-E).

440 Overall, our data show that human NT CD4 TRM share important features with mouse CD4
441 TRM, such as the expression of CD103 and CXCR6. Moreover, NT of healthy individuals is
442 populated by IAV-specific Th17 CD4 TRM.

443 ***NT Th17-CD4 TRM aid in viral clearance and dampen tissue damage***

444 Given the abundance of Th17 CD4 TRM in NT of mice and human, we wanted to further
445 delineate their functional role. First, we confirmed that PR8-infected mice carried IAV-specific
446 Th17 CD4 TRM in NT by stimulating lung and NT cells with a single immunodominant NP
447 peptide ($NP_{306-322}$) and assessing intracellular expression of IL-17a as a measure of Th17
448 response. We used $NP_{306-322}$ as this was the same peptide, loaded into tetramers, used to sort
449 CD4 TRM for scRNA sequencing. Consistent with all our data, we found that only NT, but not

450 lung, CD4 TRM from PR8 infected mice expressed IL-17a. Surprisingly, IL-17a production
451 was stimulation-independent although infection-dependent (Fig 7A-B, Fig S8A).

452 Th17 cells recruit neutrophils, B cells, promote transport of secretory IgA to the mucosal sites
453 and protect the hosts in an antibody independent manner during IAV infection(Eliasson et al.,
454 2018; Jaffar et al., 2009; Laan et al., 1999; Wang et al., 2011). On the other hand, detrimental
455 effect of Th17 was also reported as an intranasal immunization triggered Th17 population that
456 caused increased morbidity in mice(Maroof et al., 2014). To examine whether NT Th17 CD4
457 TRM had a beneficial role, we utilized $CD4^{Cre}Rorc^{fl/fl}$ (CD4-specific Th17 KO) and
458 $CD4^{Cre}Rorc^{fl/wt}$ (WT) mice(Gribonika et al., 2022) (Fig S8B). Mice deficient in *Rorc* gene lack
459 RORγt, a Th17 lineage-specific transcription factor that controls the activation of IL-17A and
460 IL-17F genes, and do not produce Th17 CD4 T cells(Ivanov et al., 2006). To verify the specific
461 role of Th17 CD4 TRM, we infected $CD4^{Cre}Rorc^{fl/fl}$ and $CD4^{Cre}Rorc^{fl/wt}$ mice with PR8 and
462 challenged them at day 30 post primary infection (Fig 7C). FTY720 treatment ruled out the
463 contribution of circulating lymphocytes. CD4 Th17 KO mice had slightly higher viral titer in
464 the NT than did WT mice on day 3 post-secondary infection (Fig. 7D). Furthermore, Th17 CD4
465 cells have been suggested to play a role in tissue repair and, by secreting anti-apoptotic
466 cytokines that dampen tissue damage(Dutta et al., 2023; Konieczny et al., 2022). We performed
467 a reinfection experiment in a similar way and enumerated apoptotic cells ($TUNEL^{+}$) in the NT
468 upon X31 challenge (Fig 7E). Indeed, $CD4^{Cre}Rorc^{fl/fl}$ mice exhibited an increased number of
469 apoptotic cells in the NT (Fig 7 F-G). However, depletion of IL-17 did not affect viral titer or
470 apoptotic cell clearance in NT (Fig S8C-D) suggesting IL-17-independent mechanisms,
471 mediated by Th17 in the NT.

472 Altogether, we confirmed that Th17 CD4 TRM ameliorate IAV-related pathology by reducing
473 viral replication and tissue damage.

474

475 **DISCUSSION**

476 The current understanding of CD4 TRM during IAV infection relies on findings from lung CD4
477 TRM. Despite the URT being the first location where IAV encounters the immune system, little
478 is known about CD4 TRM at this crucial immunological site. Here, we defined the phenotype
479 and functional role of CD4 TRM residing in the nasal tissue region of the URT. We

480 demonstrated that antigen-specific CD4 TRM vigorously respond to heterologous IAV
481 challenge, promote direct viral control and provide tissue protection in the URT.

482 Notably, we found that endogenous antigen-specific CD4 TRM, especially HA-specific ones,
483 are long lived. The HA^+ CD4 TRM in the NT decayed at a slower rate than CD4 TRMs in the
484 lungs, even though they were less abundant when quantified in absolute numbers. Furthermore,
485 a small fraction of both NP^+ and HA^+ CD4 TRM expressed Ki-67 on day 60 suggesting that
486 they may be maintained by homeostatic proliferation like lung CD4 and CD8 TRM(Takamura
487 et al., 2016; Turner et al., 2014). We hypothesize that NALT(Bates, 2022) or ectopic germinal
488 center (GC) in the NT(Gailleton et al., 2025) could be the local sites for naïve CD4 T cell
489 priming and expansion. Indeed, one recent study showed that i.n. vaccination established a CD4
490 T cell response within the interfollicular regions of the NALT, in turn promoting the homing of
491 antibody-secreting plasma cells to the NT(Liu et al., 2024). Similarly, our recent work indicated
492 that IAV infection and i.n. vaccination induce ectopic GC structures within the NT
493 itself(Gailleton et al., 2025). Furthermore, it should be noted that, while expanded lung clonal
494 families are also found within the NT, the opposite is not true, with all clonal families in the NT
495 with >8 members being organ specific (Fig 4G). However, we could not exclude the possibility
496 of some degree of replenishment from local tertiary lymphoid structures or lymphoid organs via
497 the blood. Overall, our data suggests that few cells traffic from lung draining lymph nodes to
498 NT while the majority instead expand *in situ*.

499 Even though effector T cells traffic to the infection site due to inflammatory cues, their
500 establishment as TRM may or may not require the presence of antigen depending on the tissue.
501 Antigen-dependent residency has been described for the lungs and brain(Khan et al., 2016;
502 McMaster et al., 2018; Wakim et al., 2010; Zens et al., 2016), but not genital tract or intestinal
503 CD8 TRM, where the inflammatory milieu and chemokines are sufficient for their
504 formation(Bergsbaken and Bevan, 2015; Sato et al., 2014). Even in lungs, antigen-dependency
505 can be bypassed by the introduction of adjuvants, such as zymosan, which evoke a specific
506 inflammatory milieu(Caminschi et al., 2019). Here, we demonstrated that CD4 TRM in NT
507 require the presence of cognate antigen to be formed after IAV infection, which is the opposite
508 of CD8 TRM(Pizzolla et al., 2017a). Furthermore, we showed that the same held true for lung
509 CD4 TRM. The observation in the NT highlights an interesting discrepancy regarding the

510 minimal cues needed by different T cell types to establish residency, even within the same
511 tissue.

512 Generally, CXCR6 is a chemokine receptor that is more highly expressed on CD8 T cells than
513 on CD4 T cells(Di Pilato et al., 2021; Mabrouk et al., 2022) and is well described as an essential
514 factor for CD8 TRM seeding to the lung airways but not the lung interstitium, after IAV
515 infection (Wein et al., 2019). Here, using bone marrow chimeras and blocking experiments we
516 revealed that the CXCR6-CXCL16 axis is important for the formation of antigen-specific CD4
517 TRM in NT and lungs. Another study did not find a role for CXCR6 in the recruitment of
518 antigen specific CD4 T cells to the lungs of *M. tuberculosis* infected mice (Ashhurst et al.,
519 2019), however the establishment of TRM was not verified. Nevertheless, a recent sequencing-
520 based study suggested the presence of CXCR6-CXCL16 interactions in the nasal mucosa of
521 IAV-infected mice, using cell-cell communication analysis (Kazer et al., 2024). The authors
522 showed CXCL16 to be expressed by monocyte derived macrophages and KNIIFE cells
523 (Krt13+ nasal immune-interacting floor epithelial) cells. Similarly, we found that cells in the
524 NT express CXCL16 however we did not pinpoint the specific cell population. We suggest two
525 possible mechanisms by which CXCL16 could help recruit CD4 TEM to the NT; either as
526 soluble chemokine, by attracting CD4 TEM or as membrane bound, by retaining the CD4 TRM
527 after migration (Koenen et al., 2017; Wilbanks et al., 2001). Longer depletion experiments or
528 depletion at specific time windows will help cement the role of this chemokine. Still, given the
529 homing of some CXCR6$^{-/-}$ CD4 to the NT, it is plausible that other factors may also be involved
530 in the recruitment and maintenance of TRM.

531 Functionally, NT CD4 TRM produce cytokines such as IL-2 and IFN-γ upon antigen
532 stimulation. IFN-γ is a cytokine that protects the host by inhibiting viral entry, blocking
533 attachment and replication and stimulating NK cells proliferation during the early phase of
534 infection(Brass et al., 2009; Feeley et al., 2011; Fong et al., 2022; Weiss et al., 2010). Presence
535 of TRM responding to environmental antigens, may explain cytokine production in
536 unstimulated cells. In addition, our scRNA-seq data highlighted the presence of diverse CD4
537 TRM subtypes, such as cytotoxic CD4 which has had also been suggested to play a role in
538 antiviral defense(Brown et al., 2012; McKinstry et al., 2012). In line with these mechanisms,
539 we found that CD4 TRM are essential, while circulating memory CD4 cells are dispensable, for
540 local protection in the NT. The role of NT CD4 TRM in limiting viral growth was further

541 validated by our i.t. *vs* i.n. priming model that established CD4 TRM in lungs only or in both
542 lungs and NT, respectively. Our results agree with previous work demonstrating that mucosal
543 lung CD4 TRM are better at producing IFN-γ and at protecting against IAV infection than are
544 splenic memory CD4 T cells(Teijaro et al., 2011). CTA1-3M2e-DD-vaccination provided
545 protection against viral challenge; however, the effect size was limited as the URT-restricted
546 infection was only lethal in 43% (6 of 14) of mice. In this context, it was hard to definitively
547 ascribe an effect to CD4 T cells, even if CD4 depletion resulted in a trend towards decreased
548 survival (4 of 15 mice died in CD4 depleted *vs* 1 of 15 in CTA1-3M2e-DD vaccinated). Overall,
549 we demonstrated that NT CD4 TRM have coordinated antiviral and tissue repair functions,
550 depending on antigen specificity. However, it remains to be determined how these distinct
551 protective mechanisms are integrated during a physiological, polyclonal response to infection.

552 Interestingly, we detected a greater proportion of Th17 CD4 TRM in the NT as compared to
553 lungs. Th17 enrichment was independent of both antigen specificity and infection status. In
554 general, NT harbored a substantial proportion of CD4 memory T cells and very few naïve CD4
555 T cells. Th17 cells present at steady state could have formed in response to commensal
556 microbiota of naïve mice; it is well known that commensal bacteria play an important role in
557 mucosal immunity and tolerance induction (Liu et al., 2024; Pandiyan et al., 2019). We
558 speculate that the Th17 CD4 TRM in the naïve mice might have an immunoregulatory function
559 similar to that of commensal-specific Th17 in the intestine (Brockmann et al., 2023) or that they
560 may have entered earlier in life, in response to other external stimuli. Importantly, lung Th17
561 cells have been previously reported to protect from IAV infection in an antibody independent
562 manner(Eliasson et al., 2018; Jaffar et al., 2009; Laan et al., 1999; Lin et al., 2009; McGeachy,
563 2011; Mills, 2023; Wang et al., 2011). In addition, NT Th17 cells have been shown to form
564 during and protect against several intranasal bacterial infections (Borkner et al., 2021; Solans et
565 al., 2018). All these studies took advantage of *Il17a*-/- mice, which totally lack IL-17a
566 production, and thus have not been able to determine a definitive role for CD4 Th17 cells
567 specifically. Here, we used a recently described conditional knockout, $CD4^{Cre}Rorc^{fl/fl}$
568 (Gribonika et al., 2022), which allowed us to exclusively dissect the contribution of Th17 CD4
569 T cells. We demonstrated that NT Th17 CD4 TRM play a role in reducing apoptosis and
570 somewhat in viral clearance upon heterologous IAV infection, independently of IL-17. Th17
571 CD4 T cells are also well known to produce IL-22 (Liang et al., 2006), which in turn can

572 stimulate the production of anti-apoptotic factors within airways epithelial cells and maintain a
573 healthy tissue (Omokanye et al., 2022; Sonnenberg et al., 2010). In addition, we detected IAV-
574 specific Th17 CD4 TRM in healthy human subjects, suggesting that these specific cells are
575 formed and persist in the NT of healthy adults for years and can be reactivated upon reinfection,
576 similar to what was shown for SARS-CoV-2 and *B. pertussis* (Lim et al., 2022; McCarthy et
577 al., 2024).

578 Finally, given that nasal respiratory epithelium plays a major role in the transmission of airborne
579 viruses, it is essential to focus on vaccinations that can induce memory cells in the NT(Richard
580 et al., 2020). Although the current intramuscular IAV vaccines are largely effective against IAV
581 infection, they are poor at inducing mucosal immune responses and at protecting against
582 heterologous viruses. Our findings that i.n. CTA1-3M2e-DD immunization can induce M2e-
583 specific CD4 TRM, along with another recent study showing that i.n. Spike vaccination
584 generates antigen specific CD4 TRM in the NT support i.n. immunization as an effective tool
585 for generating functional CD4 TRM in the NT(Diallo et al., 2023b). Nevertheless, immunization
586 strategies to overcome their gradual decay need to be developed.

587 Collectively, our data provide a comprehensive understanding of NT CD4 TRM that could be
588 leveraged to design mucosal vaccines aimed at generating NT CD4 TRM providing
589 heterosubtypic protection.
590

591 **MATERIALS AND METHODS**

592 **Mice**

593 We conducted the experiments according to protocols approved by regional animal ethics
594 committee in Gothenburg (ethical permit numbers: 1666/19, 2230/19 3307/20 and 38/23).
595 C57BL/6N and BALB/c mice were purchased from Janvier labs, France and Taconic
596 Biosciences, Denmark. They were housed in the specific pathogen free animal facility of
597 Experimental Biomedicine Unit (EBM) at the University of Gothenburg. B6.SJL-
598 *Ptprc*^{a} *Pepc*^{b}/BoyJ (CD45.1^{+}) and B6.129P2-*Cxcr6*^{tm1Litt}/J (*Cxcr6*$^{-/-}$) mice were purchased from
599 the Jackson Laboratory, USA and were bred at EBM. Ovalbumin-specific CD45.1^{+} OT-II,
600 tdtomato^{+} OT-II mice TCR transgenic, *CD4*^{Cre}*Rorc*$^{fl/wt}$ and *CD4*^{Cre}*Rorc*$^{fl/fl}$(Gribonika et al.,
601 2022) were bred at EBM at the University of Gothenburg. We used both female and male mice
602 which were eight to twelve weeks old in the experiments.

603 **Sampling of human subjects**

604 Written consents were obtained from the study participants before obtaining the samples.
605 Ethical permit (ethical permit number: 2023-07055-01) was obtained by the Swedish Ethical
606 Review Authority to collect paired venous blood and nasopharyngeal swabs from healthy
607 subjects aged between 18-60 years old. Both male and female volunteers were included. We
608 excluded the subjects who fulfilled any of the following criteria: respiratory infection during
609 the last two weeks, allergic rhinitis, chronic obstructive pulmonary disease, asthma, regular nose
610 bleeding, immunodeficiency and IAV infection in the last two years (verified by PCR).

611 8 ml of venous blood was collected into lithium heparin coated tubes and was subjected to
612 density gradient centrifugation to obtain peripheral blood mononuclear cells (PBMC) using
613 lymphoprep (Stemcell Technnologies) according to manufacturer's instructions.

614 Nasopharyngeal cells (NT) were collected into 3 ml RPMI containing 2% fetal calf serum
615 (FCS) and 1.5 mM DTT as previously described(Lim et al., 2022). For swab collection the
616 volunteers were seated and sample collected from both nostrils using the same Eswabs (Copan,
617 #482C). Swabs were inserted along the floor of the nasal cavity and rotated in circular motion.
618 Either posterior nasopharynx or inferior nasal turbinates were sampled from different
619 individuals. The cells were vortexed for 1 min and were incubated at 37°C for 30 min. The cells
620 were spun at 700xg for 8 min at 4°C and the cell pellets were suspended in FACS buffer.

621 In total 60 paired samples were analyzed but data from 10 of them was excluded for the
622 cytokine, CXCR6 and CD103 analysis because of low recovery of CD4 TRM from NT or
623 PBMC.

624 **Infection of mice**

625 Mouse adapted Influenza A/Puerto Rico/8/34 (PR8) (molecular clone; H1N1) and Influenza
626 A/HK/x31 (HKx31)) (molecular clone; H3N2) were grown in 10 day old embryonated chicken
627 eggs. The allantoic fluid was harvested, and the viral titer was determined using $TCID_{50}$ assay.
628 PR8 containing $OVA_{323-339}$ (PR8-OVA)(Thomas et al., 2006) was kindly gifted by Paul G.
629 Thomas, St. Jude Children's Research Hospital, USA. For sublethal total respiratory tract
630 infection (TRT infection), mice were briefly anesthetized using isoflurane and inoculated
631 intranasally with a sublethal dose (50 $TCID_{50}$) of mouse adapted Influenza A/Puerto Rico/8/34
632 (PR8) (Molecular clone; H1N1) diluted in HBSS containing 0.1% BSA (total volume of 25 µl).
633 To enhance the amount of CD4 TRM in the NT, mice were infected intranasally with a high
634 dose (10^5 $TCID_{50}$) of PR8 or PR8-OVA in a volume of 5 µl (URT restricted infection) 30
635 minutes after the TRT infection.

636 For rechallenge experiment after PR8 infection, a lethal dose of 5000 $TCID_{50}$ of X31 strain was
637 used. For rechallenge experiment after CTA1-3M2e-DD immunization, mice were infected
638 intranasally with a high dose (10^5 $TCID_{50}$) of PR8 in a volume of 10 ul in a URT restricted
639 manner.

640 For intratracheal infection, 500 $TCID_{50}$ of PR8 diluted in HBSS containing 0.1% BSA (total
641 volume of 25 µl) is inoculated intratracheally after anesthetizing the mice.

642 **Immunization of mice**

643 5µg CTA1-3M2e-DD fusion protein was diluted in 1X PBS to an end volume of 5µl. BALB/c
644 mice were immunized with CTA1-3M2e-DD intranasally and boosted twice with a ten-day
645 interval. Control group was immunized with 5µg CTA1-DD adjuvant similarly.

646 **Blocking of CXCL16, IL17A/F and depletion of T cells *in vivo***

647 Mouse CXCL16 antibody (MAB503) was purchased from R&D systems and was dissolved in
648 1X PBS. The antibody was administered intraperitoneally at a dosage of 2.5µg/g weight of
649 mouse on day 1, 3, 6 and 9 post infection with PR8. Mice treated with equal amount of

650 *InVivo*MAb rat IgG2a isotype control, anti-trinitrophenol (BE0089, Bioxcell) were used as
651 controls. For depletion of IL-17A and IL-17 F, *InVivo*MAb anti-mouse IL-17A (BE0173) and
652 *InVivo*MAb anti-mouse IL-17F (BE0303) were purchased from Bioxcell and administered
653 intraperitoneally. The mice received 400 ug of each antibody on day 29 and 200ug of each
654 antibody from day 30-32/33 post PR8 infection. The control group received equal amount of
655 *InVivo*MAb mouse IgG1 isotype control, unknown specificity (BE0083) (Bioxcell).

656 *InVivo*MAb anti-mouse CD8α (BE0117), *InVivo*MAb anti-mouse CD4 (BE0003-1) and
657 *InVivo*MAb rat IgG2b isotype control (BE0090) were purchased from Bioxcell and were
658 administered intraperitoneally at a daily dosage of 10µg/g of mouse from day 28 to day 32
659 following PR8 infection.

660 **Fingolimod treatment**

661 10mg/ml stock of fingolimod (Cayman Chemicals) was prepared in DMSO. We administrated
662 fingolimod at a dosage of 2.5 µg/g weight of mouse dissolved in sterile physiological saline
663 solution by intraperitoneal injection at indicated days.

664 **Adoptive transfer of antigen specific T cells**

665 For adoptive transfer of OT-II$^+$ CD4 T cells, CD45.1$^+$ OT-II or tdTomato$^+$ OT-II mice were
666 euthanized, and spleens were collected. Spleens were mashed and made into single cell
667 suspension by passing through a 70µm strainer. Total CD4 T cells were isolated using EasySep
668 mouse CD4$^+$ T cell isolation kit (Stemcell technologies) according to manufacturer's
669 instruction. A total of 2.5-5x10^6 OT-II$^+$ CD4 T cells suspended in 1X PBS were administrated
670 by intravenous injection four hours prior to infection with PR8-OVA.

671 For generation of effector OT-II T cells, we isolated CD4 T cells from splenocytes of tdtomato$^+$
672 OT-II mice. OT-II T cells were stimulated by culturing with splenocytes pulsed with 1uM OVA
673 peptide ISQAVHAAHAEINEAGR in 5:1 ratio respectively in RPMI media containing 10%
674 FBS, 10µg/ml gentamycin, 55µM β-mercaptoethanol (Gibco) and 20U/ml murine IL-2
675 (Peprotech) for 60h in 5% CO_2 cell culture incubator. The cells were washed and incubated with
676 fluorochrome conjugated antibodies against surface antigens- CD3 PerCPCy5.5 (17A2), CD4
677 APC-Cy7 (RM4-4) and CD69 BV605 (H1.2F3) for 20 min at 4°C. To exclude dead cells, the
678 cells were washed and stained with LIVE/DEAD™ Fixable Aqua Dead Cell Stain (cat. no:

679 L34957, Invitrogen) according to manufacturer's instruction. Cells were suspended in FACS
680 buffer and live $CD3^+CD4^+CD69^-$ $dtomato^+$ OT-II effector T cells were collected after sorting in
681 a BD FACSAria fusion (BD Biosciences). A total of $5x10^5$ effector $OT\text{-}II^+$ CD4 T cells
682 suspended in 1X PBS were administrated by intravenous injection 60 h post infection with PR8
683 or PR8-OVA.

684 **Bone marrow chimera**

685 For myeloablation, $CD45.1^+$ B6.SJL-*Ptprc*^{a} *Pepc*^{b}/BoyJ mice were irradiated with 11 Gy in
686 equally split doses with a 4-hour gap in a RS 2000 X ray irradiator machine. The mice were
687 rested for a day and transplanted with a mix of 2.5 x 10^6 $tdtomato^+$ WT and 2.5 x 10^6 $CD45.2^+$
688 *Cxcr6*-/- bone marrow cells (BM) by intravenous administration. The recipients with newly
689 reconstituted BM (BM chimera) were infected with 50 $TCID_{50}$ PR8 intravenously 70 days after
690 transplantation.

691 **Isolation and processing of blood, lungs, NALT, nasal tissue and Peyer's patches**

692 For flow cytometry experiments with cells from blood, lungs, NALT and nasal tissue, mice
693 were injected with CD4 FITC or CD4 APC-Cy7 (RM4-4) antibody intravenously to label the
694 circulating CD4 T cells. The mice were completely anesthetized, and blood was withdrawn into
695 EDTA coated tubes from the heart after five minutes of *in vivo* antibody labelling. The lung was
696 perfused with 1X PBS and processed into single cell suspension using the mouse lung
697 dissociation kit (Miltenyi Biotec). Blood was treated with RBC lysis buffer for five minutes,
698 washed and resuspended in FACS buffer. Nasal tissue and NALT were isolated and processed
699 immediately as previously described(Pizzolla et al., 2017a). For isolation of nasal tissue and
700 NALT, the mouse head was collected and deskinned. Briefly, NALT was obtained by peeling
701 the upper palate using a forceps and the cells were extracted by teasing the NALT between two
702 frosted slides. The rest of the head was cut coronally to remove the brain and the incisors were
703 removed by scissors. The nasal septum, nasoturbinates, ethmoid turbinates, vomeronasal
704 organs, olfactory recess, maxilloturbinates including cartilages and bones were collected which
705 is referred here as nasal tissue (NT). Nasal tissue was digested in 3 ml RPMI 1640 media
706 supplemented with 2% FBS, 6 mg collagenase type 3 (Worthington Biochemical corporation)
707 and 600 µg DNase I, grade II from bovine pancreas (Sigma Aldrich) in a shaking incubator at
708 37°C for one hour. The cells were made into single cell suspension by straining through a 70

709 µm nylon mesh. The cells were washed and resuspended in FACS buffer or supplemented media
710 for downstream processing.

711 For processing of cells from Peyer's patches (PPs), around 3-5 PPs were isolated from the small
712 intestine and collected in HBSS media. The PPs were washed twice with HBSS supplemented
713 with 1% FBS, 15 mM HEPES and 5 mM EDTA by incubation at 37°C for 15 min with
714 occasional shaking. The PPs were mashed, and the cells were made into single cell suspension
715 by straining through a 70 µm nylon mesh. The cells were washed and resuspended in FACS
716 buffer for staining.

717 **Stimulation of mouse cells with viral peptides**

718 The cells obtained from the organs of naïve and infected mice were stained for
719 extracellular markers prior to stimulation with peptides. The following IAV peptide array were
720 obtained from obtained from BEI resources, NIAID, NIH: Influenza Virus A/New
721 York/348/2003 (H1N1) Nucleoprotein (NP) (NR-50714), A/New York/444/2001 (H1N1)
722 Nonstructural protein 1 (NS1), Influenza Virus A/Puerto Rico/8/1934 (H1N1) Hemagglutinin
723 (HA) (NR-18973), Influenza Virus A/Puerto Rico/8/1934 (H1N1) Neuraminidase (NA) (NR-
724 19257) and SARS-Related Coronavirus 2 Nucleocapsid (N) (NR-52404). 1µg each of all
725 peptides from the peptide array were mixed to obtain the respective peptide pools.10 million
726 cells derived from lungs and nasal tissue were stimulated with IAV NP, NS1, HA and NA
727 peptide pools containing 1 µg of each peptide pool in RPMI 1640 supplemented with 10% FBS,
728 1% Penicillin/Streptomycin and Protein Transport Inhibitor (Containing Brefeldin A) (diluted
729 1:1000) (BD, 555029). The cells were incubated for four hours at 37°C and further washed with
730 1x PBS to proceed for intracellular cytokine staining.

731 For comparison of intracellular cytokines produced by CD4 TRM that are stimulated by IAV
732 NP or SARS-Related Coronavirus 2 Nucleocapsid (N) Protein (SARS-CoV-2 N), live
733 $CD3^{+}CD4iv^{-}$CD4 $tissue^{+}$ $CD44^{+}CD62L^{-}CD69^{+}$ CD4 TRM cells were sorted from lungs and NT
734 30- and 60-days post infection. The CD4 TRM ($CD45.2^{+}$) were co-cultured with congenic
735 $CD45.1^{+}$ splenocytes pulsed with IAV NP peptide pools containing 1ug of each peptide from
736 peptide array (NR-50714, BEI Resources) or with SARS-CoV-2 N peptide pools containing
737 1ug of each peptide from peptide array (NR-52404, BEI Resources) for 18 hours at 37 deg in
738 RPMI 1640 supplemented with 10% FBS, 1% Penicillin/Streptomycin. The culture was

739 supplemented with Protein Transport Inhibitor (Containing Brefeldin A) (diluted 1:1000) at the
740 12th hour. The cells were further washed with 1x PBS to proceed for intracellular cytokine
741 staining.

742 **Stimulation and flow cytometry of human PBMC and nasopharyngeal cells**

743 PBMC and NT cells were incubated with Human Trustain FcX (Biolegend, 422302) for 10 min
744 at 4°C. The cells were then incubated with anti-human CD69 BV421 antibody (clone: FNXO)
745 for 20 min at 4°C and washed with FACS buffer. The cells were finally resuspended in T cell
746 stimulation media (RPMI 1640 supplemented with 10% FBS, 1% Penicillin/Streptomycin,
747 Protein Transport Inhibitor (Containing Brefeldin A) (diluted 1:1000) (BD, 555029), Monensin
748 (Biolegend, 420701) and anti- human CD28/CD49d (BD, 347690)(Sekine et al., 2020). The
749 cells were stimulated with peptide pools containing 2ug each of all peptides from Influenza
750 Virus A/New York/348/2003 (H1N1) Nucleoprotein (NP) (NR-50714) peptide array and
751 Influenza Virus A/New York/348/2003 (H1N1) Matrix protein 1 (M1) (NR-2613) peptide array
752 for 6 hours at 37°C. Cells without the peptide pools (peptide diluent) were kept as unstimulated
753 controls. After washing with FACS buffer, the cells were stained for extracellular antigens with
754 the following fluorochrome conjugated antibodies (clone used indicated in bracket): anti-CD3
755 BUV737 (UCHT1), anti-CD4 PE-Dazzle594 (OKT4), anti-CD45RA BV605 (HI100), anti-
756 CCR7 APC-Cy7 (G043H7), anti-CD103 FITC (Ber-ACT8) and anti-CXCR6 (13B1E5). After
757 incubation at 4°C for 20 min, the cells were washed and stained with LIVE/DEAD™ Fixable
758 Aqua Dead Cell Stain (cat. no: L34957, Invitrogen) according to manufacturer's instruction to
759 exclude dead cells. To detect intracellular cytokines, the cells were fixed with 4%
760 paraformaldehyde for 20 min at RT, washed with ice cold 1X PBS and permeabilized with
761 permeabilization buffer (1X PBS containing 0.5% BSA and 0.5% saponin) for 10 min at RT.
762 The cells were washed and resuspended in permeabilization buffer with the following
763 fluorochrome conjugated antibody cocktail: anti- IFN-γ PE (25723.11), anti-TNF BV650
764 (MAb11) and anti-IL-17a APC (BL168). After incubation at 4°C overnight, the cells were
765 washed and suspended in FACS buffer for data acquisition at BD LSR Fortessa X-20 or Sony
766 spectral analyzer.

767 **Flow cytometry of murine cells**

768 All fluorochrome-conjugated antibodies are titrated to determine the optimal concentration for
769 flow cytometry. Single cell suspension from organs were prepared and resuspended in FACS
770 buffer as mentioned before. The following antibodies are used for mouse extracellular antigen
771 staining: anti-CD3 PerCPCy5.5 (17A2), anti-CD4 FITC (RM4-4), anti-CD4 APC-Cy7 and
772 BUV496 (RM4-5), anti-CD8 PE-Cy7 (53-6.7) anti-CD44 BV786 (IM7), anti-CD44 PE-Dazzle
773 594 (IM7), anti-CD62L BV711 and APC (MEL-14), anti-CD69 BUV737 (H1.2F3), anti-
774 CD11a PE-Cy7 (H155-78), anti-CD103 PE-Cy7, BV421 and BV711 (2E7), anti-CD45.1 APC
775 (A20), anti-CD45.2 BUV395 (104), anti-CXCR6 BV421 (SA051D1), anti-ICOS BV421
776 (7E.17G9), anti-PD1 PE (J43), anti-CD19-Alexa Flour 700 (6D5), anti-CD11b-Alexa Flour 700
777 (M1/70). The extracellular staining was performed by incubating the cells with the antibodies
778 for 20 minutes at 4°C. For labelling antigen specific cells with fluorochrome conjugated
779 tetramers, cells were incubated with the tetramers for 2h 40 min at 4°C (I-A^b $NP_{306-322}$ APC and
780 I-A^b HA_{91-107} PE/BV421 tetramers) or 1 h at room temperature (I-A^d $M2e_{2-17}$ PE) and the
781 extracellular antibody mix was added onto the top and incubated for 20 minutes. The following
782 tetramers kindly provided by NIH tetramer core facility at Emory University were used: I-A^b
783 $NP_{306-322}$ APC, I-A^d $M2e_{2-17}$ PE, I-Ab HA_{91-107} PE and I-Ab HA_{91-107} BV421. I-A^b human
784 $CLIP_{87-101}$ conjugated with APC, PE or BV421 and I-A^d human CLIP $_{87-101}$ conjugated with PE
785 were used as negative controls. To exclude dead cells, the cells were washed and stained with
786 LIVE/DEAD™ Fixable Aqua Dead Cell Stain (cat. no: L34957, Invitrogen) according to
787 manufacturer's instruction. The cells were fixed with IC fixation buffer (eBioscience, 00-8222)
788 for intracellular cytokine staining, or fixed with Foxp3 Transcription Factor
789 Fixation/Permeabilization buffer (eBioscience 00-5523) for transcription factor staining for 60
790 minutes at room temperature. The cells were washed and resuspended in 1X permeabilization
791 buffer (eBioscience, 00-8333) and incubated with the following antibodies: anti-IL-2 BV785
792 (JES6-5H4), anti-TNF BV421 (MP6-XT22), anti-IFN-γ BV605 (XMG1.2), anti-IL-17a PE or
793 FITC (TC11-18H10), anti-RORγt PE-CF594 (Q31-378) and anti-Ki-67 V450 (B56). The cells
794 were washed with 1X permeabilization buffer and resuspended in FACS buffer. The labelled
795 cells were run, and the data was acquired on the BD LSR Fortessa X-20 or BD LSR II (BD
796 Biosciences) flow cytometer or Sony ID7000 Spectral cell analyzer and was analyzed using
797 Flow-Jo software (Tree Star).

798 **Immunofluorescence staining**

799 Mice were euthanized and upper part of mice heads were collected after removing the skin and
800 eyeballs. The heads were fixed with 1.5% Formaldehyde Solution (w/v) (ThermoScientific)
801 solution at 4°C for 24 hours. After removing the teeth and remaining muscle tissues, they were
802 transferred into 0.5M EDTA solution for decalcification for 7 days at 4°C. The samples were
803 embedded into sequential dilutions of OCT paramount (Histolab) and were snap frozen for
804 sectioning. 10-14 µm thick frontal sections thick sections were cut and SuperFrost microscopy
805 slides and stored at -80°C or were processed for staining. In the latter case, slides were baked
806 for 1 hour at 60°C. Antigen retrieval was performed on nasal tissue sections mounted on glass
807 slides to enhance epitope accessibility for immunofluorescence staining. Slides were submerged
808 in a sodium citrate retrieval buffer consisting of 10 mM sodium citrate and 0.05% Tween-20,
809 adjusted to pH 6.0. Heat-induced epitope retrieval was carried out by placing the slides in the
810 buffer and heating them in a microwave until the solution reached 100 °C. Once the target
811 temperature was reached, the slides were removed from heat and allowed to cool gradually to
812 room temperature for approximately 1 hour. Following cooling, slides were fixed with ice-cold
813 acetone until the samples were dried. The tissue was blocked with 1X PBS containing 10% FBS
814 and 5% Normal Rat Serum for 15 min at RT. After washing with 1X PBS, the tissues were
815 stained with antibody cocktail overnight at 4°C in the dark. The following antibodies were used:
816 anti-CXCL16 (Uncoupled Polyclonal, #bs-1441R-TR Biosciences), anti-CD4 (FITC RM4-4,
817 #116004 Biolegend), anti-CD44 (APC IM7, #103012 Biolegend), anti-CD45.1 (PE A20,
818 #110707 Biolegend), Goat anti-Rabbit IgG (Texas Red, #sc-2780 Santa Cruz Biotech).The
819 sections were counterstained by incubating with Hoechst 33342 solution (ThermoFischer
820 Scientific) for 15 min at RT in the dark. The sections were mounted with a fluorescent mounting
821 medium (Dako), acquired on an Axio Imager. Z2 (Zeiss) and analysed on TissueFACS Analyser
822 (Version 7.1.120 Xylis).

823 **TUNEL assay**

824 Mice were euthanized and upper part of mice heads were collected after removing the skin and
825 eyeballs. The heads were fixed with 4% Formaldehyde Solution (w/v) (ThermoScientific)
826 solution at 4°C for 24 hours. After removing the teeth and remaining muscle tissues, they were
827 transferred into 14% EDTA solution (w/v) for decalcification for 14 days at 4°C. The tissues
828 were sequentially dehydrated and embedded into paraffin wax in a cassette. 4 µm thick sections
829 were cut from the paraffinized tissue blocks. TUNEL assay kit -HRP-DAB (Abcam, ab206386)

830 was used to detect apoptotic cells according to manufacturer´s instructions. The images were
831 Axio Imager. Z2 (Zeiss) and analysed on TissueFACS Analyser (Version 7.1.120 Xylis) and
832 QuPath (version 0.5.1) software.

833 **Neutralization assay**

834 200000 MDCK cells were plated in a 24 well plate and was incubated overnight at 37°C. Serum
835 from IAV infected mice or mice immunized with irrelevant protein (streptavidin or SARS-CoV-
836 2 spike protein) was serially diluted (two-fold) and incubated with 10^6 $TCID_{50}$ X31 (MOI=5)
837 in 500µl DMEM supplemented with 1mM HEPES, 1µg/ml TPCK trypsin and 5µg/ml
838 gentamycin for 1 hour at 37°C. The plate containing MDCK cells was washed twice with 1x
839 PBS and the virus/serum mixture was added onto the cells. The plate was incubated for 18 hours
840 and washed twice with 1x PBS. The cells were incubated with 5x trypsin for cell detachment
841 and the washed cells were fixed with fixation/permeabilization solution (eBioscience™ Foxp3
842 / Transcription Factor Staining Buffer Set, 00-5523-00) overnight at 4°C. The cells were washed
843 twice with FACS buffer containing 0.1% saponin. The infected cells were labelled by
844 incubating cells with InVivoMAb anti-Influenza A virus NP (clone H16-L10-4R5 (HB65))
845 (Bioxcell) labelled with alexa fluor 488 (Protein Labeling Kits for alexafluor 488, Invitrogen,
846 A10235) for 30 minutes at 4°C. The cells were washed twice with FACS buffer containing 0.1%
847 saponin and resuspended in FACS buffer for flow cytometry. The average signals from cells
848 incubated with virus in the absence of serum was considered as 100% infectivity and is used to
849 calculate the relative infectivity of cells in presence of serum.

850 **Viral titer determination**

851 Lung and URT (nasal tissue and NALT) are harvested and suspended in 1ml 1x PBS per 0.5g
852 of organ. The tissues were homogenized using a tissue homogenizer and spun at 1200xg for 10
853 min at 4°C. The supernatant was used for determining the viral titer using the standard $TCID_{50}$
854 assay.

855 **Single cell RNA sequencing**

856 Mice were injected with CD4 FITC (RM4-4) antibody intravenously to label the circulating
857 CD4 T cells (referred as CD4 iv). The mice were completely anesthetized, and the lung was
858 perfused with 1X PBS. Nasal tissue and lungs were isolated, digested and processed into single

859 cells as described before. The samples were enriched for CD4 T cells using the EasySep™
860 mouse CD4+ T Cell isolation kit (Stemcell technologies) and the dead cells were removed using
861 EasySep™ Dead Cell Removal (Annexin V) Kit (Stemcell technologies) according to
862 manufacturer's instruction. Cells from PR8 infected mice were labelled with the following
863 fluorochrome-conjugated MHC-II tetramers: I-Ab $NP_{306-322}$ APC and I-Ab HA_{91-107} BV421 as
864 described before. After washing with FACS buffer, cells were labelled with TotalSeq™-C0987
865 anti-APC antibody (408007, Biolegend) to identify NP-specific CD4 TRM. Cells were washed
866 and labelled with antibodies. The following fluorochrome labelled antibodies were used: CD3
867 PerCPCy5.5 (17A2), CD4 APC-Cy7 (RM4-4) (for labelling tissue resident CD4 Tc- referred as
868 CD4 tissue) and CD69 BV605 (H1.2F3) and CD44 PE-Dazzle 594 (IM7) and CD62L BV711
869 (MEL-14). Additionally, totalSeq-C0595 anti-mouse CD11a antibody (101131, Biolegend) and
870 the following barcoded hashtag antibodies were used: hashtag antibodies 3,5-9 (155865,
871 155869, 155871, 155873, 155875, 155877; Biolegend) for demultiplexing of samples during
872 data processing and to detect cells expressing CD11a protein on the cell surface. Live total CD4
873 TRM (CD4 iv^- CD4 $tissue^+CD44^+CD62L^-CD69^+$) were sorted from PR8 infected and naïve
874 mice while NP-specific CD4 TRM ($NP_{306-322}^+$ CD4 iv^- CD4 $tissue^+CD44^+CD62L^-CD69^+$) and
875 HA-specific CD4 TRM (HA_{91-107}^+ CD4 iv^- CD4 $tissue^+CD44^+CD62L^-CD69^+$) were sorted from
876 PR8 infected mice. In addition to CD4 T cells, we sorted total live cells devoid of CD4 T cells
877 from the NT of naïve and PR8 infected mice. The sorted cells were collected in a BD FACSAria
878 fusion (BD Biosciences) cell sorter and processed immediately. The total number of cells sorted
879 from each group are the following. Lung total CD4 TRM from naïve mice: 8000 cells, NT total
880 CD4 TRM from naïve mice: 3095 cells, lung NP-specific CD4 TRM: 4002 cells, NT NP-
881 specific CD4 TRM: 1172 cells, lung HA-specific CD4 TRM: 4073 cells, NT HA-specific CD4
882 TRM: 1314 cells, lung total CD4 TRM from infected mice: 8000 cells, NT total CD4 TRM
883 from infected mice: 3000 cells, live cells except CD4 T cells from NT of naïve and infected
884 mice: 10000 cells each. The sorted cells were pooled and washed in the Laminar Wash Mini
885 system (Curiox Biosystems).

886 A maximum of 20,000 cells were processed into single cells in a chromium controller (10X
887 Genomics). The single cell gene expression, TCR VDJ and cell surface protein (CSP) libraries
888 were prepared using Chromium Next GEM Single Cell 5' Reagent Kits v2 (Dual Index) kit (PN-
889 1000265), library construction kit (PN-1000190), 5' Feature Barcode Kit (PN-1000256),

890 Chromium Single Cell Mouse TCR Amplification Kit (PN-1000254), Chromium Next GEM
891 Chip K Single Cell Kit (1000286), Dual Index Kit TT Set A (PN-1000215) and Dual Index Kit
892 TN Set A (PN-1000250). The prepared cDNA libraries were quantified using Qubit
893 Fluorometer (Invitrogen) and quality was assessed using Agilent Tapestation system. The
894 libraries were sequenced on Illumina NovaSeq 6000 by SNP&SEQ Technology Platform,
895 Science for Life Laboratory (Uppsala Biomedical Centre, Uppsala University, Sweden)
896 according to sequencing instructions provided by 10x Genomics.

897 **Single cell RNA seq data processing**

898 Raw fastq files were processed through the 10X cellranger pipeline using the multi command
899 and default parameters with reference genome GRCm38-mm10. Raw UMI count matrices
900 generated from the cellranger 10X pipeline were loaded and merged into a single Seurat object
901 (Seurat version 4)(Hao et al., 2021; Hao et al., 2024; Satija et al., 2015). Cells were discarded
902 if they met any of the following criteria: percentage of mitochondrial counts > 15%, number of
903 unique features or total counts was in the bottom or top 0.5% of all cells, and number of unique
904 features < 250. Gene counts were normalized to the same total counts per cell and were natural
905 log transformed (after the addition of a pseudocount of 1). The normalized counts in each cell
906 were mean-centered and scaled by their SD, and the following variables were regressed out:
907 percentage of mitochondrial counts, percentage of ribosomal counts, G2M and S phase scores,
908 TCR gene expression scores. Hashtags and APC-surface antibody were normalized by a
909 centered log-ratio (CLR) normalization and binding assigned using HTODemux function. Data
910 integration across cells originating from different samples was done using the Anchor method
911 within Seurat. Selection of the number of components for the nearest-neighbor network
912 computation was based on their visualization in an elbow plot. UMAP(Becht et al., 2018) was
913 performed for the spatial visualization of the single-cell data set after features and cells were
914 clustered using the Louvain algorithm. TCR data was processed using scRepertoire
915 package(Borcherding et al., 2020) with standard setting. T cell clonality was based on identical
916 nucleotide sequence in the CDR3 region. All TCR information were integrated with the scRNA-
917 Seq data by aligning and merging the data with the metadata slot in the processed RNA-Seq
918 Seurat object. Differentially expressed genes between different clusters were identified using
919 the FindAllMarkers function from Seurat using default settings (Wilcoxon test and Bonferroni
920 P value correction). Significant genes with average log fold change > 0.25 and expressed in >

921 25% of cells in that group were ranked according to fold change and are reported in table S1.
922 For comparison between 2 groups, the FindMarkers function was used, and either top and
923 bottom 20 genes were represented by Heatmap using the DoHeatmap function of Seurat or all
924 genes were represented on a VolcanoPlot using the EnhancedVolcano R package(Blighe K,
925 2024). Data underlying the volcano plot is in Table S1. Gene signatures were added to the Seurat
926 object using the AddModuleScore function.

927 **Statistical analysis**

928 The data was analyzed using GraphPad prism software. The experiments were performed and
929 analyzed in a non-blinded fashion. Both male and female mice were included in the
930 experiments. For statistical analysis, unpaired two-tailed *t*-test, one-way ANOVA, with
931 Dunnet's multiple comparison test, two-way ANOVA, Tukey's multiple comparison test or
932 two-sided Wilcoxon matched-pairs signed-rank test and is indicated in the figure legends.
933 Normality and lognormality was tested using GraphPad prism. Differences were considered
934 significant when the P-value was <0.05. Outliers were identified and removed using Grubbs
935 method (alpha=0.05) when indicated in the figure legend. For weight loss analysis, we used a
936 linear mixed effects analysis of the body weight data (normalized to the initial weight of each
937 individual animal) in R (www.r-project.org). As fixed effects, we used the treatment and the
938 day (with an interaction term between those fixed effects). As random effects we had intercepts
939 for the individual animals. Thereafter, we compared the weight curves across treatment groups
940 (averaged over time) using estimated marginal means and pairwise comparisons with Tukey's
941 Honest Significant Difference (HSD) adjustment. To assess treatment group differences at each
942 time point, we used the same linear mixed-effects model described above. Estimated marginal
943 means were computed for each treatment group at each individual day (0–14). Pairwise
944 comparisons between treatment groups were performed at each time point, and p-values were
945 adjusted for multiple testing using Holm's method.

946 **Acknowledgments:**

947 We would like to thank the staff at the Experimental Biomedicine (EBM) core facility at the
948 University of Gothenburg for animal management; Paul G. Thomas, St. Jude Children's hospital
949 for PR8-OVA virus; Linda M Wakim, Doherty Institute for providing protocol for processing
950 of nasal tissue; Carina Karlsson, University of Gothenburg for providing access to microtome;

Alvar Almstedt, Bioinformatics and Data Centre (BDC), Core Facilities, University of Gothenburg, for data pre-processing; Genomics core facility at Sahlgrenska Hospital for providing access to Qubit fluorometer and tapestation and study participants for providing samples. MHC-II tetramers were obtained from the NIH tetramer core facility. The following reagents were obtained through BEI Resources, NIAID, NIH: Peptide Array, Influenza Virus A/New York/348/2003 (H1N1) Nucleocapsid Protein, NR-5071, Peptide Array, Influenza Virus A/New York/348/2003 (H1N1) Matrix protein 1 (M1) (NR-2613) and Peptide Array, SARS-Related Coronavirus 2 Nucleocapsid (N) Protein (NR-52404). Sequencing was performed by the SNP&SEQ Technology Platform in Uppsala. The facility is part of the National Genomics Infrastructure (NGI) Sweden and Science for Life Laboratory. The SNP&SEQ Platform is also supported by the Swedish Research Council and the Knut and Alice Wallenberg Foundation. The experiment schemes are created with Biorender.com.

Funding:

The project was supported by grants from the European Research Council (ERC-StG, B-DOMINANCE, grant no. 850638 to DA); the Swedish Research Council (grant no. 2021-01164, 2021-01165 to DA); the Knut and Alice Wallenberg Foundation (grant no 2021.0033 and 2024.0097 to DA) and the Sahlgrenska Academy (GU2020/2376-JNR2020 to DA). NRM is supported by Svenska Sällskapet för Medicinsk Forskning post-doctoral grant (grant no: PD20-0017), Elisabeth Bollan Linden stipend, Stiftelsen Lars Hiertas Minne and Stiftelsen Wilhelm och Martina Lundgrens Vetenskapsfond. KT is supported by grants from Svenska Sällskapet för Medicinsk Forskning (S21-0083).

Author contributions:

Conceptualization: NRM, DA. Methodology: NRM, RG, LS, KS, AS, MB, KT, DA. Formal analysis: NRM, RG, LS, KS, JE, HA, AS, NL, MB, KT, DA. Investigation: NRM, RG, LS, KS, JE, HA, MB, KT, DA. Data curation: DA, NRM. Software: DA, NRM. Resources: NL, MB. Project Administration: NRM, DA. Supervision: MB, NL, KT, DA. Funding Acquisition: DA, NRM. Writing – original draft: NRM, DA. Writing – review & editing: NRM, RG, LS, KS, JE, HA, AS, MB, KT, DA.

Competing interests:

The authors have no conflicts of interest to disclose.

981 **Data availability**

982 Single-cell RNA-seq data have been deposited in the NCBI GEO database under accession
983 number []. All other data are present in the article and Supplementary Information.

984

985 **REFERENCES**

986

987 Andreatta, M., A. Tjitropranoto, Z. Sherman, M.C. Kelly, T. Ciucci, and S.J. Carmona. 2022. A CD4(+) T cell
988 reference map delineates subtype-specific adaptation during acute and chronic viral infections. *eLife* 11:
989 Ashhurst, A.S., M. Flórido, L.C.W. Lin, D. Quan, E. Armitage, S.A. Stifter, J. Stambas, and W.J. Britton. 2019.
990 CXCR6-Deficiency Improves the Control of Pulmonary Mycobacterium tuberculosis and Influenza
991 Infection Independent of T-Lymphocyte Recruitment to the Lungs. *Frontiers in immunology* 10:339.
992 Bates, J.T. 2022. Naïve CD4(+) T Cell Activation in the Nasal-Associated Lymphoid Tissue following Intranasal
993 Immunization with a Flagellin-Based Subunit Vaccine. *International journal of molecular sciences* 23:
994 Becht, E., L. McInnes, J. Healy, C.A. Dutertre, I.W.H. Kwok, L.G. Ng, F. Ginhoux, and E.W. Newell. 2018.
995 Dimensionality reduction for visualizing single-cell data using UMAP. *Nature biotechnology*
996 Bergsbaken, T., and M.J. Bevan. 2015. Proinflammatory microenvironments within the intestine regulate the
997 differentiation of tissue-resident $CD8^+$ T cells responding to infection. *Nature immunology* 16:406-414.
998 Besavilla, D.F., L. Reusch, J. Enriquez, K. Schon, and D. Angeletti. 2023. Pre-existing CD4 T cell help boosts
999 antibody responses but has limited impact on germinal center, antigen-specific B cell frequencies after
1000 influenza infection. *Front Immunol* 14:1243164.
1001 Beura, L.K., N.J. Fares-Frederickson, E.M. Steinert, M.C. Scott, E.A. Thompson, K.A. Fraser, J.M. Schenkel, V.
1002 Vezys, and D. Masopust. 2019. CD4(+) resident memory T cells dominate immunosurveillance and
1003 orchestrate local recall responses. *The Journal of experimental medicine* 216:1214-1229.
1004 Blighe K, R.S., Lewis M 2024. EnhancedVolcano: Publication-ready volcano plots with enhanced colouring and
1005 labeling, R package version 1.22.0,https://github.com/kevinblighe/EnhancedVolcano.
1006 Bodewes, R., G. de Mutsert, F.R. van der Klis, M. Ventresca, S. Wilks, D.J. Smith, M. Koopmans, R.A.
1007 Fouchier, A.D. Osterhaus, and G.F. Rimmelzwaan. 2011. Prevalence of antibodies against seasonal
1008 influenza A and B viruses in children in Netherlands. *Clin Vaccine Immunol* 18:469-476.
1009 Borcherding, N., N.L. Bormann, and G. Kraus. 2020. scRepertoire: An R-based toolkit for single-cell immune
1010 receptor analysis. *F1000Research* 9:47.
1011 Borkner, L., L.M. Curham, M.M. Wilk, B. Moran, and K.H.G. Mills. 2021. IL-17 mediates protective immunity
1012 against nasal infection with Bordetella pertussis by mobilizing neutrophils, especially Siglec-F(+)
1013 neutrophils. *Mucosal immunology* 14:1183-1202.
1014 Brass, A.L., I.C. Huang, Y. Benita, S.P. John, M.N. Krishnan, E.M. Feeley, B.J. Ryan, J.L. Weyer, L. van der
1015 Weyden, E. Fikrig, D.J. Adams, R.J. Xavier, M. Farzan, and S.J. Elledge. 2009. The IFITM proteins
1016 mediate cellular resistance to influenza A H1N1 virus, West Nile virus, and dengue virus. *Cell*
1017 139:1243-1254.
1018 Brinkmann, V., M.D. Davis, C.E. Heise, R. Albert, S. Cottens, R. Hof, C. Bruns, E. Prieschl, T. Baumruker, P.
1019 Hiestand, C.A. Foster, M. Zollinger, and K.R. Lynch. 2002. The immune modulator FTY720 targets
1020 sphingosine 1-phosphate receptors. *The Journal of biological chemistry* 277:21453-21457.
1021 Brockmann, L., A. Tran, Y. Huang, M. Edwards, C. Ronda, H.H. Wang, and Ivanov, II. 2023. Intestinal
1022 microbiota-specific Th17 cells possess regulatory properties and suppress effector T cells via c-MAF
1023 and IL-10. *Immunity* 56:2719-2735.e2717.
1024 Brown, D.M., S. Lee, L. Garcia-Hernandez Mde, and S.L. Swain. 2012. Multifunctional CD4 cells expressing
1025 gamma interferon and perforin mediate protection against lethal influenza virus infection. *Journal of*
1026 *virology* 86:6792-6803.
1027 Brownlie, D., I. Rødahl, R. Varnaite, H. Asgeirsson, H. Glans, S. Falck-Jones, S. Vangeti, M. Buggert, H.G.
1028 Ljunggren, J. Michaëlsson, S. Gredmark-Russ, A. Smed-Sörensen, and N. Marquardt. 2022.
1029 Comparison of Lung-Homing Receptor Expression and Activation Profiles on NK Cell and T Cell
1030 Subsets in COVID-19 and Influenza. *Frontiers in immunology* 13:834862.

1031 Caminschi, I., M.H. Lahoud, A. Pizzolla, and L.M. Wakim. 2019. Zymosan by-passes the requirement for
1032 pulmonary antigen encounter in lung tissue-resident memory CD8(+) T cell development. *Mucosal*
1033 *immunology* 12:403-412.
1034 Campbell, A.P., C. Ogokeh, J.Y. Lively, M.A. Staat, R. Selvarangan, N.B. Halasa, J.A. Englund, J.A. Boom,
1035 G.A. Weinberg, J.V. Williams, M. McNeal, C.J. Harrison, L.S. Stewart, E.J. Klein, L.C. Sahni, P.G.
1036 Szilagyi, M.G. Michaels, R.W. Hickey, M.E. Moffat, B.A. Pahud, J.E. Schuster, G.M. Weddle, B. Rha,
1037 A.M. Fry, and M. Patel. 2020. Vaccine Effectiveness Against Pediatric Influenza Hospitalizations and
1038 Emergency Visits. *Pediatrics* 146:
1039 Cohen, N.R., P.J. Brennan, T. Shay, G.F. Watts, M. Brigl, J. Kang, and M.B. Brenner. 2013. Shared and distinct
1040 transcriptional programs underlie the hybrid nature of iNKT cells. *Nature immunology* 14:90-99.
1041 Devaiah, B.N., H. Lu, A. Gegonne, Z. Sercan, H. Zhang, R.J. Clifford, M.P. Lee, and D.S. Singer. 2010. Novel
1042 functions for TAF7, a regulator of TAF1-independent transcription. *The Journal of biological chemistry*
1043 285:38772-38780.
1044 Dey, S., H. Ashwin, L. Milross, B. Hunter, J. Majo, A.J. Filby, A.J. Fisher, P.M. Kaye, and D. Lagos. 2023.
1045 Downregulation of MALAT1 is a hallmark of tissue and peripheral proliferative T cells in COVID-19.
1046 *Clinical and experimental immunology* 212:262-275.
1047 Di Pilato, M., R. Kfuri-Rubens, J.N. Pruessmann, A.J. Ozga, M. Messemaker, B.L. Cadilha, R. Sivakumar, C.
1048 Cianciaruso, R.D. Warner, F. Marangoni, E. Carrizosa, S. Lesch, J. Billingsley, D. Perez-Ramos, F.
1049 Zavala, E. Rheinbay, A.D. Luster, M.Y. Gerner, S. Kobold, M.J. Pittet, and T.R. Mempel. 2021.
1050 CXCR6 positions cytotoxic T cells to receive critical survival signals in the tumor microenvironment.
1051 *Cell* 184:4512-4530.e4522.
1052 Diallo, B.K., N.C. C, T.Y. Wong, P. Schmitt, K.S. Lee, K. Weaver, O. Miller, M. Cooper, S.D. Jazayeri, F.H.
1053 Damron, and K.H.G. Mills. 2023a. Intranasal COVID-19 vaccine induces respiratory memory T cells
1054 and protects K18-hACE mice against SARS-CoV-2 infection. *NPJ vaccines* 8:68.
1055 Diallo, B.K., C. Ní Chasaide, T.Y. Wong, P. Schmitt, K.S. Lee, K. Weaver, O. Miller, M. Cooper, S.D. Jazayeri,
1056 F.H. Damron, and K.H.G. Mills. 2023b. Intranasal COVID-19 vaccine induces respiratory memory T
1057 cells and protects K18-hACE mice against SARS-CoV-2 infection. *NPJ vaccines* 8:68.
1058 Dutta, A., C.Y. Hung, T.C. Chen, S.H. Hsiao, C.S. Chang, Y.C. Lin, C.Y. Lin, and C.T. Huang. 2023. An IL-17-
1059 EGFR-TRAF4 axis contributes to the alleviation of lung inflammation in severe influenza.
1060 *Communications biology* 6:600.
1061 Eliasson, D.G., K. El Bakkouri, K. Schön, A. Ramne, E. Festjens, B. Löwenadler, W. Fiers, X. Saelens, and N.
1062 Lycke. 2008. CTA1-M2e-DD: a novel mucosal adjuvant targeted influenza vaccine. *Vaccine* 26:1243-
1063 1252.
1064 Eliasson, D.G., A. Omokanye, K. Schon, U.A. Wenzel, V. Bernasconi, M. Bemark, A. Kolpe, K. El Bakkouri, T.
1065 Ysenbaert, L. Deng, W. Fiers, X. Saelens, and N. Lycke. 2018. M2e-tetramer-specific memory CD4 T
1066 cells are broadly protective against influenza infection. *Mucosal immunology* 11:273-289.
1067 Feeley, E.M., J.S. Sims, S.P. John, C.R. Chin, T. Pertel, L.M. Chen, G.D. Gaiha, B.J. Ryan, R.O. Donis, S.J.
1068 Elledge, and A.L. Brass. 2011. IFITM3 inhibits influenza A virus infection by preventing cytosolic
1069 entry. *PLoS pathogens* 7:e1002337.
1070 Fong, C.H., L. Lu, L.L. Chen, M.L. Yeung, A.J. Zhang, H. Zhao, K.Y. Yuen, and K.K. To. 2022. Interferon-
1071 gamma inhibits influenza A virus cellular attachment by reducing sialic acid cluster size. *iScience*
1072 25:104037.
1073 Gailleton, R., N.R. Mathew, L. Reusch, K. Schon, L. Scharf, A. Stromberg, A. Cvjetkovic, L. Aziz, J. Hellgren,
1074 K.W. Tang, M. Bemark, and D. Angeletti. 2025. Ectopic germinal centers in the nasal turbinates
1075 contribute to B cell immunity to intranasal viral infection and vaccination. *Proc Natl Acad Sci U S A*
1076 122:e2421724122.
1077 Goplen, N.P., Y. Wu, Y.M. Son, C. Li, Z. Wang, I.S. Cheon, L. Jiang, B. Zhu, K. Ayasoufi, E.N. Chini, A.J.
1078 Johnson, R. Vassallo, A.H. Limper, N. Zhang, and J. Sun. 2020. Tissue-resident CD8(+) T cells drive
1079 age-associated chronic lung sequelae after viral pneumonia. *Science immunology* 5:
1080 Gribonika, I., A. Stromberg, C. Lebrero-Fernandez, K. Schon, J. Moon, M. Bemark, and N. Lycke. 2022. Peyer's
1081 patch T(H)17 cells are dispensable for gut IgA responses to oral immunization. *Sci Immunol*
1082 7:eabc5500.
1083 Hao, Y., S. Hao, E. Andersen-Nissen, W.M. Mauck, 3rd, S. Zheng, A. Butler, M.J. Lee, A.J. Wilk, C. Darby, M.
1084 Zager, P. Hoffman, M. Stoeckius, E. Papalexi, E.P. Mimitou, J. Jain, A. Srivastava, T. Stuart, L.M.
1085 Fleming, B. Yeung, A.J. Rogers, J.M. McElrath, C.A. Blish, R. Gottardo, P. Smibert, and R. Satija.
1086 2021. Integrated analysis of multimodal single-cell data. *Cell* 184:3573-3587.e3529.

1087 Hao, Y., T. Stuart, M.H. Kowalski, S. Choudhary, P. Hoffman, A. Hartman, A. Srivastava, G. Molla, S. Madad,
1088 C. Fernandez-Granda, and R. Satija. 2024. Dictionary learning for integrative, multimodal and scalable
1089 single-cell analysis. *Nature biotechnology* 42:293-304.
1090 Hashimoto, K., T. Kouno, T. Ikawa, N. Hayatsu, Y. Miyajima, H. Yabukami, T. Terooatea, T. Sasaki, T. Suzuki,
1091 M. Valentine, G. Pascarella, Y. Okazaki, H. Suzuki, J.W. Shin, A. Minoda, I. Taniuchi, H. Okano, Y.
1092 Arai, N. Hirose, and P. Carninci. 2019. Single-cell transcriptomics reveals expansion of cytotoxic CD4
1093 T cells in supercentenarians. *Proc Natl Acad Sci U S A* 116:24242-24251.
1094 Hoft, S.G., M.A. Sallin, K.D. Kauffman, S. Sakai, V.V. Ganusov, and D.L. Barber. 2019. The Rate of CD4 T
1095 Cell Entry into the Lungs during Mycobacterium tuberculosis Infection Is Determined by Partial and
1096 Opposing Effects of Multiple Chemokine Receptors. *Infection and immunity* 87:
1097 Hu, X., M. Wu, T. Ma, Y. Zhang, C. Zou, R. Wang, Y. Zhang, Y. Ren, Q. Li, H. Liu, H. Li, T. Wang, X. Sun, Y.
1098 Yang, M. Tang, X. Li, J. Li, X. Gao, T. Li, and X. Zhou. 2022. Single-cell transcriptomics reveals
1099 distinct cell response between acute and chronic pulmonary infection of Pseudomonas aeruginosa.
1100 *MedComm* 3:e193.
1101 Ivanov, II, B.S. McKenzie, L. Zhou, C.E. Tadokoro, A. Lepelley, J.J. Lafaille, D.J. Cua, and D.R. Littman. 2006.
1102 The orphan nuclear receptor RORgammat directs the differentiation program of proinflammatory IL-
1103 17+ T helper cells. *Cell* 126:1121-1133.
1104 Jaffar, Z., M.E. Ferrini, L.A. Herritt, and K. Roberts. 2009. Cutting edge: lung mucosal Th17-mediated responses
1105 induce polymeric Ig receptor expression by the airway epithelium and elevate secretory IgA levels.
1106 *Journal of immunology (Baltimore, Md. : 1950)* 182:4507-4511.
1107 Kazer, S.W., C.M. Match, E.M. Langan, M.-A. Messou, T.J. LaSalle, E. O'Leary, J. Marbourg, K. Naughton,
1108 U.H. von Andrian, and J. Ordovas-Montanes. 2024. Primary nasal influenza infection rewires the tissue-
1109 scale memory response dynamics. *Immunity*
1110 Khan, T.N., J.L. Mooster, A.M. Kilgore, J.F. Osborn, and J.C. Nolz. 2016. Local antigen in nonlymphoid tissue
1111 promotes resident memory CD8+ T cell formation during viral infection. *The Journal of experimental*
1112 *medicine* 213:951-966.
1113 Kinnear, E., L. Lambert, J.U. McDonald, H.M. Cheeseman, L.J. Caproni, and J.S. Tregoning. 2018. Airway T
1114 cells protect against RSV infection in the absence of antibody. *Mucosal immunology* 11:249-256.
1115 Koenen, A., A. Babendreyer, J. Schumacher, T. Pasqualon, N. Schwarz, A. Seifert, X. Deupi, A. Ludwig, and D.
1116 Dreymueller. 2017. The DRF motif of CXCR6 as chemokine receptor adaptation to adhesion. *PloS one*
1117 12:e0173486.
1118 Konieczny, P., Y. Xing, I. Sidhu, I. Subudhi, K.P. Mansfield, B. Hsieh, D.E. Biancur, S.B. Larsen, M. Cammer,
1119 D. Li, N.X. Landén, C. Loomis, A. Heguy, A.N. Tikhonova, A. Tsirigos, and S. Naik. 2022. Interleukin-
1120 17 governs hypoxic adaptation of injured epithelium. *Science (New York, N.Y.)* 377:eabg9302.
1121 Kourepini, E., M. Aggelakopoulou, T. Alissafi, N. Paschalidis, D.C. Simoes, and V. Panoutsakopoulou. 2014.
1122 Osteopontin expression by CD103- dendritic cells drives intestinal inflammation. *Proc Natl Acad Sci U*
1123 *S A* 111:E856-865.
1124 Künzli, M., and D. Masopust. 2023. CD4(+) T cell memory. *Nature immunology* 24:903-914.
1125 Kurd, N.S., Z. He, T.L. Louis, J.J. Milner, K.D. Omilusik, W. Jin, M.S. Tsai, C.E. Widjaja, J.N. Kanbar, J.G.
1126 Olvera, T. Tysl, L.K. Quezada, B.S. Boland, W.J. Huang, C. Murre, A.W. Goldrath, G.W. Yeo, and J.T.
1127 Chang. 2020. Early precursors and molecular determinants of tissue-resident memory CD8(+) T
1128 lymphocytes revealed by single-cell RNA sequencing. *Science immunology* 5:
1129 Laan, M., Z.H. Cui, H. Hoshino, J. Lötvall, M. Sjöstrand, D.C. Gruenert, B.E. Skoogh, and A. Lindén. 1999.
1130 Neutrophil recruitment by human IL-17 via C-X-C chemokine release in the airways. *Journal of*
1131 *immunology (Baltimore, Md. : 1950)* 162:2347-2352.
1132 Li, J., E. Lu, T. Yi, and J.G. Cyster. 2016. EBI2 augments Tfh cell fate by promoting interaction with IL-2-
1133 quenching dendritic cells. *Nature* 533:110-114.
1134 Liang, S.C., X.Y. Tan, D.P. Luxenberg, R. Karim, K. Dunussi-Joannopoulos, M. Collins, and L.A. Fouser. 2006.
1135 Interleukin (IL)-22 and IL-17 are coexpressed by Th17 cells and cooperatively enhance expression of
1136 antimicrobial peptides. *The Journal of experimental medicine* 203:2271-2279.
1137 Lim, J.M.E., A.T. Tan, N. Le Bert, S.K. Hang, J.G.H. Low, and A. Bertoletti. 2022. SARS-CoV-2 breakthrough
1138 infection in vaccinees induces virus-specific nasal-resident CD8+ and CD4+ T cells of broad specificity.
1139 *J Exp Med* 219:
1140 Lin, Y., S. Ritchea, A. Logar, S. Slight, M. Messmer, J. Rangel-Moreno, L. Guglani, J.F. Alcorn, H. Strawbridge,
1141 S.M. Park, R. Onishi, N. Nyugen, M.J. Walter, D. Pociask, T.D. Randall, S.L. Gaffen, Y. Iwakura, J.K.

1142 Kolls, and S.A. Khader. 2009. Interleukin-17 is required for T helper 1 cell immunity and host
1143 resistance to the intracellular pathogen Francisella tularensis. *Immunity* 31:799-810.
1144 Liu, J., L. Stoler-Barak, H. Hezroni-Bravyi, A. Biram, S. Lebon, N. Davidzohn, M. Kedmi, M. Chemla, D.
1145 Pilzer, M. Cohen, O. Brenner, M. Biton, and Z. Shulman. 2024. Turbinate-homing IgA-secreting cells
1146 originate in the nasal lymphoid tissues. *Nature* 632:637-646.
1147 Mabrouk, N., T. Tran, I. Sam, I. Pourmir, N. Gruel, C. Granier, J. Pineau, A. Gey, S. Kobold, E. Fabre, and E.
1148 Tartour. 2022. CXCR6 expressing T cells: Functions and role in the control of tumors. *Frontiers in*
1149 *immunology* 13:1022136.
1150 Marchesini Tovar, G., C. Gallen, and T. Bergsbaken. 2024. CD8+ Tissue-Resident Memory T Cells: Versatile
1151 Guardians of the Tissue. *Journal of immunology (Baltimore, Md. : 1950)* 212:361-368.
1152 Maroof, A., Y.M. Yorgensen, Y. Li, and J.T. Evans. 2014. Intranasal vaccination promotes detrimental Th17-
1153 mediated immunity against influenza infection. *PLoS pathogens* 10:e1003875.
1154 Mas-Orea, X., L. Rey, L. Battut, C. Bories, C. Petitfils, A. Abot, N. Gheziel, E. Wemelle, C. Blanpied, J.P.
1155 Motta, C. Knauf, F. Barreau, E. Espinosa, M. Aloulou, N. Cenac, M. Serino, L. Mouledous, N.
1156 Fazilleau, and G. Dietrich. 2023. Proenkephalin deletion in hematopoietic cells induces intestinal barrier
1157 failure resulting in clinical feature similarities with irritable bowel syndrome in mice. *Communications*
1158 *biology* 6:1168.
1159 McCarthy, K.N., S. Hone, R.M. McLoughlin, and K.H.G. Mills. 2024. IL-17 and IFN-γ-producing respiratory
1160 tissue resident memory CD4 T cells persist for decades in adults immunized as children with whole cell
1161 pertussis vaccines. *The Journal of infectious diseases*
1162 McGeachy, M.J. 2011. GM-CSF: the secret weapon in the T(H)17 arsenal. *Nature immunology* 12:521-522.
1163 McKinstry, K.K., T.M. Strutt, Y. Kuang, D.M. Brown, S. Sell, R.W. Dutton, and S.L. Swain. 2012. Memory
1164 CD4+ T cells protect against influenza through multiple synergizing mechanisms. *The Journal of*
1165 *clinical investigation* 122:2847-2856.
1166 McMaster, S.R., A.N. Wein, P.R. Dunbar, S.L. Hayward, E.K. Cartwright, T.L. Denning, and J.E. Kohlmeier.
1167 2018. Pulmonary antigen encounter regulates the establishment of tissue-resident CD8 memory T cells
1168 in the lung airways and parenchyma. *Mucosal immunology* 11:1071-1078.
1169 Miller, I., M. Min, C. Yang, C. Tian, S. Gookin, D. Carter, and S.L. Spencer. 2018. Ki67 is a Graded Rather than
1170 a Binary Marker of Proliferation versus Quiescence. *Cell Rep* 24:1105-1112.e1105.
1171 Miller, M.A., A.P. Ganesan, N. Luckashenak, M. Mendonca, and L.C. Eisenlohr. 2015. Endogenous antigen
1172 processing drives the primary CD4+ T cell response to influenza. *Nature medicine* 21:1216-1222.
1173 Mills, K.H.G. 2023. IL-17 and IL-17-producing cells in protection versus pathology. *Nature reviews.*
1174 *Immunology* 23:38-54.
1175 Moguche, A.O., S. Shafiani, C. Clemons, R.P. Larson, C. Dinh, L.E. Higdon, C.J. Cambier, J.R. Sissons, A.M.
1176 Gallegos, P.J. Fink, and K.B. Urdahl. 2015. ICOS and Bcl6-dependent pathways maintain a CD4 T cell
1177 population with memory-like properties during tuberculosis. *The Journal of experimental medicine*
1178 212:715-728.
1179 Ng, S.S., F. De Labastida Rivera, J. Yan, D. Corvino, I. Das, P. Zhang, R. Kuns, S.B. Chauhan, J. Hou, X.Y. Li,
1180 T.C.M. Frame, B.A. McEnroe, E. Moore, J. Na, J.A. Engel, M.S.F. Soon, B. Singh, A.J. Kueh, M.J.
1181 Herold, M. Montes de Oca, S.S. Singh, P.T. Bunn, A.R. Aguilera, M. Casey, M. Braun, N. Ghazanfari,
1182 S. Wani, Y. Wang, F.H. Amante, C.L. Edwards, A. Haque, W.C. Dougall, O.P. Singh, A.G. Baxter,
1183 M.W.L. Teng, A. Loukas, N.L. Daly, N. Cloonan, M.A. Degli-Esposti, J. Uzonna, W.R. Heath, T. Bald,
1184 S.K. Tey, K. Nakamura, G.R. Hill, R. Kumar, S. Sundar, M.J. Smyth, and C.R. Engwerda. 2024. Author
1185 Correction: The NK cell granule protein NKG7 regulates cytotoxic granule exocytosis and
1186 inflammation. *Nature immunology* 25:716.
1187 Nguyen, K.D., A. Fohner, J.D. Booker, C. Dong, A.M. Krensky, and K.C. Nadeau. 2008. XCL1 enhances
1188 regulatory activities of CD4+ CD25(high) CD127(low/-) T cells in human allergic asthma. *Journal of*
1189 *immunology (Baltimore, Md. : 1950)* 181:5386-5395.
1190 O'Hara, J.M., N.S. Redhu, E. Cheung, N.G. Robertson, I. Patik, S.E. Sayed, C.M. Thompson, M. Herd, K.B.
1191 Lucas, E. Conaway, C.C. Morton, D.L. Farber, R. Malley, and B.H. Horwitz. 2020. Generation of
1192 protective pneumococcal-specific nasal resident memory CD4(+) T cells via parenteral immunization.
1193 *Mucosal immunology* 13:172-182.
1194 Omokanye, A., L.C. Ong, C. Lebrero-Fernandez, V. Bernasconi, K. Schon, A. Stromberg, M. Bemark, X.
1195 Saelens, P. Czarnewski, and N. Lycke. 2022. Clonotypic analysis of protective influenza M2e-specific
1196 lung resident Th17 memory cells reveals extensive functional diversity. *Mucosal immunology* 15:717-
1197 729.

1198 Paget, J., P. Spreeuwenberg, V. Charu, R.J. Taylor, A.D. Iuliano, J. Bresee, L. Simonsen, and C. Viboud. 2019.
1199 Global mortality associated with seasonal influenza epidemics: New burden estimates and predictors
1200 from the GLaMOR Project. *Journal of global health* 9:020421.
1201 Pandiyan, P., N. Bhaskaran, M. Zou, E. Schneider, S. Jayaraman, and J. Huehn. 2019. Microbiome Dependent
1202 Regulation of T(regs) and Th17 Cells in Mucosa. *Frontiers in immunology* 10:426.
1203 Peng, C., M.A. Huggins, K.M. Wanhainen, T.P. Knutson, H. Lu, H. Georgiev, K.L. Mittelsteadt, N.N. Jarjour, H.
1204 Wang, K.A. Hogquist, D.J. Campbell, H. Borges da Silva, and S.C. Jameson. 2022. Engagement of the
1205 costimulatory molecule ICOS in tissues promotes establishment of CD8(+) tissue-resident memory
1206 T cells. *Immunity* 55:98-114.e115.
1207 Pizzolla, A., T.H.O. Nguyen, J.M. Smith, A.G. Brooks, K. Kedzieska, W.R. Heath, P.C. Reading, and L.M.
1208 Wakim. 2017a. Resident memory CD8(+) T cells in the upper respiratory tract prevent pulmonary
1209 influenza virus infection. *Sci Immunol* 2:
1210 Pizzolla, A., Z. Wang, J.R. Groom, K. Kedzierska, A.G. Brooks, P.C. Reading, and L.M. Wakim. 2017b. Nasal-
1211 associated lymphoid tissues (NALTs) support the recall but not priming of influenza virus-specific
1212 cytotoxic T cells. *Proc Natl Acad Sci U S A* 114:5225-5230.
1213 Plasek, L.M., and S. Valadkhan. 2021. lncRNAs in T lymphocytes: RNA regulation at the heart of the immune
1214 response. *American journal of physiology. Cell physiology* 320:C415-c427.
1215 Ramirez, S.I., F. Faraji, L.B. Hills, P.G. Lopez, B. Goodwin, H.D. Stacey, H.J. Sutton, K.M. Hastie, E.O.
1216 Saphire, H.J. Kim, S. Mashoof, C.H. Yan, A.S. DeConde, G. Levi, and S. Crotty. 2024. Immunological
1217 memory diversity in the human upper airway. *Nature* 632:630-636.
1218 Randall, T.D. Structure, Organization, and Development of the Mucosal Immune System of the Respiratory
1219 Tract. Mucosal Immunology. 2015:43-61. doi: 10.1016/B978-0-12-415847-4.00004-5. Epub 2015 Mar
1220 13.,
1221 Rauen, T., C.M. Hedrich, K. Tenbrock, and G.C. Tsokos. 2013. cAMP responsive element modulator: a critical
1222 regulator of cytokine production. *Trends in molecular medicine* 19:262-269.
1223 Richard, M., J.M.A. van den Brand, T.M. Bestebroer, P. Lexmond, D. de Meulder, R.A.M. Fouchier, A.C.
1224 Lowen, and S. Herfst. 2020. Influenza A viruses are transmitted via the air from the nasal respiratory
1225 epithelium of ferrets. *Nature communications* 11:766.
1226 Satija, R., J.A. Farrell, D. Gennert, A.F. Schier, and A. Regev. 2015. Spatial reconstruction of single-cell gene
1227 expression data. *Nature biotechnology* 33:495-502.
1228 Sato, A., A. Suwanto, M. Okabe, S. Sato, T. Nochi, T. Imai, N. Koyanagi, J. Kunisawa, Y. Kawaguchi, and H.
1229 Kiyono. 2014. Vaginal memory T cells induced by intranasal vaccination are critical for protective T
1230 cell recruitment and prevention of genital HSV-2 disease. *Journal of virology* 88:13699-13708.
1231 Sekine, T., A. Perez-Potti, O. Rivera-Ballesteros, K. Strålin, J.B. Gorin, A. Olsson, S. Llewellyn-Lacey, H.
1232 Kamal, G. Bogdanovic, S. Muschiol, D.J. Wullimann, T. Kammann, J. Emgård, T. Parrot, E. Folkesson,
1233 O. Rooyackers, L.I. Eriksson, J.I. Henter, A. Sönnerborg, T. Allander, J. Albert, M. Nielsen, J.
1234 Klingström, S. Gredmark-Russ, N.K. Björkström, J.K. Sandberg, D.A. Price, H.G. Ljunggren, S.
1235 Aleman, and M. Buggert. 2020. Robust T Cell Immunity in Convalescent Individuals with
1236 Asymptomatic or Mild COVID-19. *Cell* 183:158-168.e114.
1237 Shiow, L.R., D.B. Rosen, N. Brdicková, Y. Xu, J. An, L.L. Lanier, J.G. Cyster, and M. Matloubian. 2006. CD69
1238 acts downstream of interferon-alpha/beta to inhibit S1P1 and lymphocyte egress from lymphoid organs.
1239 *Nature* 440:540-544.
1240 Solans, L., A.S. Debrie, L. Borkner, N. Aguiló, A. Thiriard, L. Coutte, S. Uranga, F. Trottein, C. Martín, K.H.G.
1241 Mills, and C. Locht. 2018. IL-17-dependent SIgA-mediated protection against nasal Bordetella pertussis
1242 infection by live attenuated BPZE1 vaccine. *Mucosal immunology* 11:1753-1762.
1243 Son, Y.M., I.S. Cheon, Y. Wu, C. Li, Z. Wang, X. Gao, Y. Chen, Y. Takahashi, Y.X. Fu, A.L. Dent, M.H.
1244 Kaplan, J.J. Taylor, W. Cui, and J. Sun. 2021. Tissue-resident CD4(+) T helper cells assist the
1245 development of protective respiratory B and CD8(+) T cell memory responses. *Science immunology* 6:
1246 Sonnenberg, G.F., M.G. Nair, T.J. Kirn, C. Zaph, L.A. Fouser, and D. Artis. 2010. Pathological versus protective
1247 functions of IL-22 in airway inflammation are regulated by IL-17A. *The Journal of experimental*
1248 *medicine* 207:1293-1305.
1249 Swarnalekha, N., D. Schreiner, L.C. Litzler, S. Iftikhar, D. Kirchmeier, M. Kunzli, Y.M. Son, J. Sun, E.A.
1250 Moreira, and C.G. King. 2021. T resident helper cells promote humoral responses in the lung. *Sci*
1251 *Immunol* 6:

1252 Szabo, P.A., H.M. Levitin, M. Miron, M.E. Snyder, T. Senda, J. Yuan, Y.L. Cheng, E.C. Bush, P. Dogra, P.
1253 Thapa, D.L. Farber, and P.A. Sims. 2019a. Single-cell transcriptomics of human T cells reveals tissue
1254 and activation signatures in health and disease. *Nature communications* 10:4706.
1255 Szabo, P.A., M. Miron, and D.L. Farber. 2019b. Location, location, location: Tissue resident memory T cells in
1256 mice and humans. *Science immunology* 4:
1257 Takamura, S., H. Yagi, Y. Hakata, C. Motozono, S.R. McMaster, T. Masumoto, M. Fujisawa, T. Chikaishi, J.
1258 Komeda, J. Itoh, M. Umemura, A. Kyusai, M. Tomura, T. Nakayama, D.L. Woodland, J.E. Kohlmeier,
1259 and M. Miyazawa. 2016. Specific niches for lung-resident memory CD8+ T cells at the site of tissue
1260 regeneration enable CD69-independent maintenance. *The Journal of experimental medicine* 213:3057-
1261 3073.
1262 Teijaro, J.R., D. Turner, Q. Pham, E.J. Wherry, L. Lefrancois, and D.L. Farber. 2011. Cutting edge: Tissue-
1263 retentive lung memory CD4 T cells mediate optimal protection to respiratory virus infection. *Journal of*
1264 *immunology (Baltimore, Md. : 1950)* 187:5510-5514.
1265 The, L. 2024. H5N1: international failures and uncomfortable truths. *Lancet (London, England)* 403:2455.
1266 Thomas, P.G., S.A. Brown, W. Yue, J. So, R.J. Webby, and P.C. Doherty. 2006. An unexpected antibody
1267 response to an engineered influenza virus modifies CD8+ T cell responses. *Proc Natl Acad Sci U S A*
1268 103:2764-2769.
1269 Thome, J.J., N. Yudanin, Y. Ohmura, M. Kubota, B. Grinshpun, T. Sathaliyawala, T. Kato, H. Lerner, Y. Shen,
1270 and D.L. Farber. 2014. Spatial map of human T cell compartmentalization and maintenance over
1271 decades of life. *Cell* 159:814-828.
1272 Tuomela, K., A.R. Ambrose, and D.M. Davis. 2022. Escaping Death: How Cancer Cells and Infected Cells
1273 Resist Cell-Mediated Cytotoxicity. *Frontiers in immunology* 13:867098.
1274 Turner, D.L., K.L. Bickham, J.J. Thome, C.Y. Kim, F. D'Ovidio, E.J. Wherry, and D.L. Farber. 2014. Lung
1275 niches for the generation and maintenance of tissue-resident memory T cells. *Mucosal immunology*
1276 7:501-510.
1277 Uddbäck, I., S.E. Michalets, A. Saha, C. Mattingly, K.N. Kost, M.E. Williams, L.A. Lawrence, S.L. Hicks, A.C.
1278 Lowen, H. Ahmed, A.R. Thomsen, C.J. Russell, C.D. Scharer, J.M. Boss, K. Koelle, R. Antia, J.P.
1279 Christensen, and J.E. Kohlmeier. 2024. Prevention of respiratory virus transmission by resident memory
1280 CD8(+) T cells. *Nature* 626:392-400.
1281 Vijayanand, S., K.B. Gomes, R.P. Gala, M.N. Uddin, and M.J. D'Souza. 2020. Exploring the Potential of T-Cells
1282 for a Universal Influenza Vaccine. *Vaccines* 8:
1283 Wakim, L.M., A. Woodward-Davis, and M.J. Bevan. 2010. Memory T cells persisting within the brain after local
1284 infection show functional adaptations to their tissue of residence. *Proc Natl Acad Sci U S A* 107:17872-
1285 17879.
1286 Wang, X., C.C. Chan, M. Yang, J. Deng, V.K. Poon, V.H. Leung, K.H. Ko, J. Zhou, K.Y. Yuen, B.J. Zheng, and
1287 L. Lu. 2011. A critical role of IL-17 in modulating the B-cell response during H5N1 influenza virus
1288 infection. *Cellular & molecular immunology* 8:462-468.
1289 Wang, X., X. Shen, S. Chen, H. Liu, N. Hong, H. Zhong, X. Chen, and W. Jin. 2022. Reinvestigation of Classic
1290 T Cell Subsets and Identification of Novel Cell Subpopulations by Single-Cell RNA Sequencing.
1291 *Journal of immunology (Baltimore, Md. : 1950)* 208:396-406.
1292 Wang, Z., S. Wang, N.P. Goplen, C. Li, I.S. Cheon, Q. Dai, S. Huang, J. Shan, C. Ma, Z. Ye, M. Xiang, A.H.
1293 Limper, E.C. Porquera, J.E. Kohlmeier, M.H. Kaplan, N. Zhang, A.J. Johnson, R. Vassallo, and J. Sun.
1294 2019. PD-1(hi) CD8(+) resident memory T cells balance immunity and fibrotic sequelae. *Science*
1295 *immunology* 4:
1296 Wein, A.N., S.R. McMaster, S. Takamura, P.R. Dunbar, E.K. Cartwright, S.L. Hayward, D.T. McManus, T.
1297 Shimaoka, S. Ueha, T. Tsukui, T. Masumoto, M. Kurachi, K. Matsushima, and J.E. Kohlmeier. 2019.
1298 CXCR6 regulates localization of tissue-resident memory CD8 T cells to the airways. *The Journal of*
1299 *experimental medicine* 216:2748-2762.
1300 Weiss, I.D., O. Wald, H. Wald, K. Beider, M. Abraham, E. Galun, A. Nagler, and A. Peled. 2010. IFN-gamma
1301 treatment at early stages of influenza virus infection protects mice from death in a NK cell-dependent
1302 manner. *Journal of interferon & cytokine research : the official journal of the International Society for*
1303 *Interferon and Cytokine Research* 30:439-449.
1304 Wilbanks, A., S.C. Zondlo, K. Murphy, S. Mak, D. Soler, P. Langdon, D.P. Andrew, L. Wu, and M. Briskin.
1305 2001. Expression cloning of the STRL33/BONZO/TYMSTRligand reveals elements of CC, CXC, and
1306 CX3C chemokines. *Journal of immunology (Baltimore, Md. : 1950)* 166:5145-5154.

1307 Wimmers, F., A.R. Burrell, Y. Feng, H. Zheng, P.S. Arunachalam, M. Hu, S. Spranger, L.E. Nyhoff, D. Joshi,
1308 M. Trisal, M. Awasthi, L. Bellusci, U. Ashraf, S. Kowli, K.C. Konvinse, E. Yang, M. Blanco, K.
1309 Pellegrini, G. Tharp, T. Hagan, R.S. Chinthrajah, T.T. Nguyen, A. Grifoni, A. Sette, K.C. Nadeau, D.B.
1310 Haslam, S.E. Bosinger, J. Wrammert, H.T. Maecker, P.J. Utz, T.T. Wang, S. Khurana, P. Khatri, M.A.
1311 Staat, and B. Pulendran. 2023. Multi-omics analysis of mucosal and systemic immunity to SARS-CoV-
1312 2 after birth. *Cell* 186:4632-4651.e4623.
1313 Woodring, T., C.N. Dewey, L.D. Santos Dias, X. He, H.E. Dobson, M. Wüthrich, and B. Klein. 2022. Distinctive
1314 populations of CD4(+)T cells associated with vaccine efficacy. *iScience* 25:104934.
1315 Xu, Q., P. Milanez-Almeida, A.J. Martins, A.J. Radtke, K.B. Hoehn, C. Oguz, J. Chen, C. Liu, J. Tang, G.
1316 Grubbs, S. Stein, S. Ramelli, J. Kabat, H. Behzadpour, M. Karkanitsa, J. Spathies, H. Kalish, L.
1317 Kardava, M. Kirby, F. Cheung, S. Preite, P.C. Duncker, M.M. Kitakule, N. Romero, D. Preciado, L.
1318 Gitman, G. Koroleva, G. Smith, A. Shaffer, I.T. McBain, P.J. McGuire, S. Pittaluga, R.N. Germain, R.
1319 Apps, D.M. Schwartz, K. Sadtler, S. Moir, D.S. Chertow, S.H. Kleinstein, S. Khurana, J.S. Tsang, P.
1320 Mudd, P.L. Schwartzberg, and K. Manthiram. 2023. Adaptive immune responses to SARS-CoV-2
1321 persist in the pharyngeal lymphoid tissue of children. *Nature immunology* 24:186-199.
1322 Yan, Y., G.X. Zhang, M.S. Williams, G.B. Carey, H. Li, J. Yang, A. Rostami, and H. Xu. 2012. TCR stimulation
1323 upregulates MS4a4B expression through induction of AP-1 transcription factor during T cell activation.
1324 *Molecular immunology* 52:71-78.
1325 Yang, H.Q., Y.S. Wang, K. Zhai, and Z.H. Tong. 2021. Single-Cell TCR Sequencing Reveals the Dynamics of T
1326 Cell Repertoire Profiling During Pneumocystis Infection. *Frontiers in microbiology* 12:637500.
1327 Yount, K.S., J.M. Hall, K. Caution, M.M. Shamseldin, M. Guo, K. Marion, A.R. Fullen, Y. Huang, J.A.
1328 Maynard, S.A. Quataert, R. Deora, and P. Dubey. 2023. Systemic priming and intranasal booster with a
1329 BcfA-adjuvanted acellular pertussis vaccine generates CD4+ IL-17+ nasal tissue resident T cells and
1330 reduces B. pertussis nasal colonization. *Frontiers in immunology* 14:1181876.
1331 Zens, K.D., J.K. Chen, and D.L. Farber. 2016. Vaccine-generated lung tissue-resident memory T cells provide
1332 heterosubtypic protection to influenza infection. *JCI insight* 1:
1333 Zens, K.D., J.K. Chen, R.S. Guyer, F.L. Wu, F. Cvetkovski, M. Miron, and D.L. Farber. 2017. Reduced
1334 generation of lung tissue-resident memory T cells during infancy. *The Journal of experimental medicine*
1335 214:2915-2932.
1336 Zheng, M.Z.M., T.K. Tan, F. Villalon-Letelier, H. Lau, Y.M. Deng, S. Fritzlar, S.A. Valkenburg, H. Gu, L.L.M.
1337 Poon, P.C. Reading, A.R. Townsend, and L.M. Wakim. 2023. Single-cycle influenza virus vaccine
1338 generates lung CD8(+) Trm that cross-react against viral variants and subvert virus escape mutants.
1339 *Science advances* 9:eadg3469.

1340
1341

FIGURES

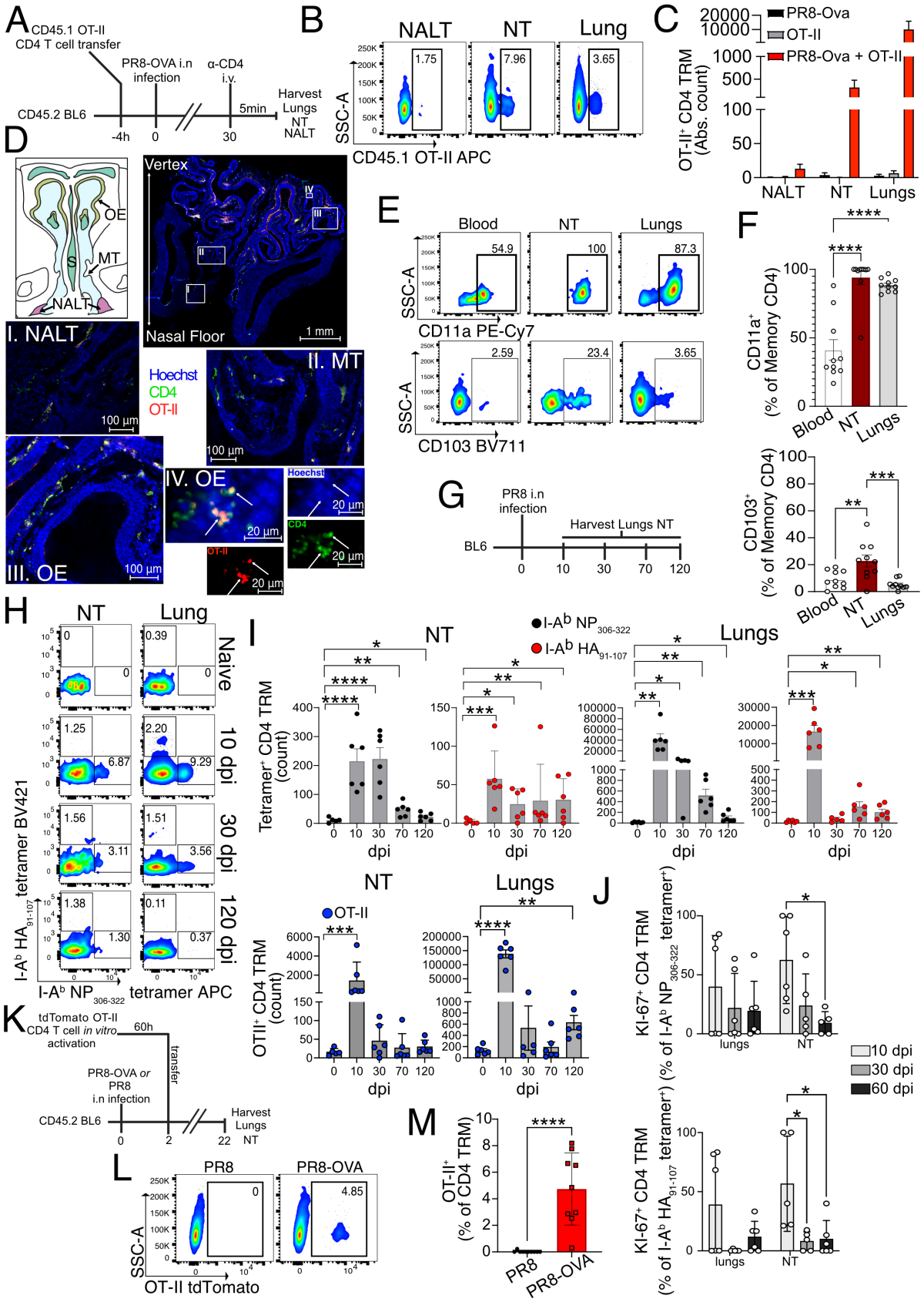
A
CD45.1 OT-II
CD4 T cell transfer
PR8-OVA i.n
infection
α-CD4
i.v.
5min
Harvest
Lungs
NT
NALT
CD45.2 BL6
-4h
0
30
B
NALT
NT
Lung
1.75
7.96
3.65
SSC-A
CD45.1 OT-II APC
C
PR8-Ova
OT-II
PR8-Ova + OT-II
OT-II+ CD4 TRM
(Abs. count)
NALT
NT
Lungs
D
OE
MT
NALT
Vertex
Nasal Floor
1 mm
I. NALT
II. MT
III. OE
IV. OE
Hoechst
CD4
OT-II
100 µm
20 µm
E
Blood
NT
Lungs
54.9
100
87.3
2.59
23.4
3.65
SSC-A
CD11a PE-Cy7
CD103 BV711
F
CD11a+
(% of Memory CD4)
CD103+
(% of Memory CD4)
Blood
NT
Lungs
G
PR8 i.n
infection
Harvest Lungs NT
BL6
0
10
30
70
120
H
NT
Lung
Naive
10 dpi
30 dpi
120 dpi
0
0.39
1.25
6.87
2.20
9.29
1.56
3.11
1.51
3.56
1.38
1.30
0.11
0.37
I-Ab HA91-107 tetramer BV421
I-Ab NP306-322 tetramer APC
I
I-Ab NP306-322
I-Ab HA91-107
NT
Lungs
Tetramer+ CD4 TRM
(count)
dpi
OT-II
OTII+ CD4 TRM
(count)
J
KI-67+ CD4 TRM
(% of I-Ab NP306-322 tetramer+)
KI-67+ CD4 TRM
(% of I-Ab HA91-107 tetramer+)
lungs
NT
10 dpi
30 dpi
60 dpi
K
tdTomato OT-II
CD4 T cell in vitro
activation
60h
transfer
PR8-OVA or
PR8
i.n infection
CD45.2 BL6
Harvest
Lungs
NT
0
2
22
L
PR8
PR8-OVA
0
4.85
SSC-A
OT-II tdTomato
M
OT-II+
(% of CD4 TRM)
PR8
PR8-OVA

Fig 1: IAV-specific CD4 TRM are formed at the URT and is dependent on presence of cognate antigen

A) Schematic diagram showing the procedure of transfer of OVA specific (OT-II) CD4 T cells, infection of mice with PR8-OVA and subsequent harvesting of organs.

B-C) CD45.1$^+$ or tdtomato$^+$ OT-II CD4 TRM (gated on live CD3$^+$CD4iv$^-$CD4 tissue$^+$CD44$^+$CD62L$^-$CD69$^+$ as shown in Fig S1A) in different organs of CD45.2$^+$ recipients on day 30 following PR8-OVA infection. B) Representative flow cytometry plots indicating the percentages of CD45.1$^+$ OT-II CD4 TRM. The data are representative of one experiment out of three independent experiments. C) Bar graph indicating the absolute number of CD45.1$^+$ or tdtomato$^+$ OT-II CD4 TRM. The experiment was repeated thrice and the results (mean ± s.e.m.) were pooled.

D) Representative microscopic images of OT-II$^+$ (red) CD4$^+$ (green) T cells in different sections of the NT and NALT. The sections are derived from day 30 following PR8-OVA infection of mice that received OT-II CD4 T cells as described in fig. 1 A. Scale bars are indicated in each image. MT= Maxilloturbinate, OE= Olfactory epithelium, S= Nasal septum.

E-F) Frequency of CD103$^+$ and CD11a$^+$ cells among OT-II CD4 TRM in NT and lungs (gated on live CD3$^+$CD4iv$^-$CD4 tissue$^+$CD44$^+$CD62L$^-$CD69$^+$), and among total CD4 effector memory T cells (CD3$^+$CD4 iv$^+$CD44$^+$CD62L$^-$) in blood of CD45.2$^+$ recipients on day 30 following IAV infection. E) Representative flow cytometry plots indicating the percentages of CD103$^+$ and CD11a$^+$ cells. The data is representative of one experiment out of two independent experiments. F) Scatter plot indicating the percentages of CD103$^+$ and CD11a$^+$ cells. Each data point indicates an individual mouse. The experiment was repeated twice and the results (mean ± s.e.m.) were pooled. NS, not significant, ****P<0.0001; ***P<0.001; **P<0.01; *P<0.05 by one-way ANOVA, with Dunnet's multiple comparison test.

G-I) Kinetics of I-A^b NP$_{306-322}$ tetramer, I-A^b HA$_{91-107}$ tetramer- specific CD4 TRM and OT-II$^+$ CD4 TRM in the NT and lungs on indicated days following PR8-OVA IAV infection. G) Schematic representation of the experimental setup. H) Representative flow cytometry plots indicating the percentages of I-A^b NP$_{306-322}$ tetramer and I-A^b HA$_{91-107}$ tetramer- specific CD4 TRM are shown. I) Scatter plot indicating the absolute numbers of I-A^b NP$_{306-322}$ tetramer, I-A^b HA$_{91-107}$ tetramer- specific CD4 TRM and OT-II$^+$ CD4 TRM. Each data point indicates an individual mouse. The experiment was performed once and the results (mean ± s.e.m.) were plotted. NS, not significant, ****P<0.0001; ***P<0.001; **P<0.01; *P<0.05 by lognormal one-way ANOVA.

J) Scatter plot showing the percentage of Ki-67$^+$ cells among I-A^b NP$_{306-322}$ tetramer$^+$ and I-A^b HA$_{91-107}$ tetramer$^+$ CD4 TRM in lung and NT isolated on day 10, 30 and 60 post PR8 infection. The experiment was performed twice, and the results (mean ± s.e.m.) were pooled. NS, not significant, ****P<0.0001; ***P<0.001; **P<0.01; *P<0.05 by two-way ANOVA, with Tukey's multiple comparison test.

K-M) Frequency of OT-II CD4 TRM in the NT on day 22 following infection with PR8 or PR8-OVA. K) Schematic representation of the experimental setup. L) A representative flow cytometry plot indicating the frequency of OT-II CD4 TRM. M) Scatter plot showing the frequency of OT-II CD4 TRM. The experiment was performed twice and the results (mean ± s.e.m.) are pooled. NS, not significant, ****P<0.0001; ***P<0.001; **P<0.01; *P<0.05 by unpaired two-tailed t-test.

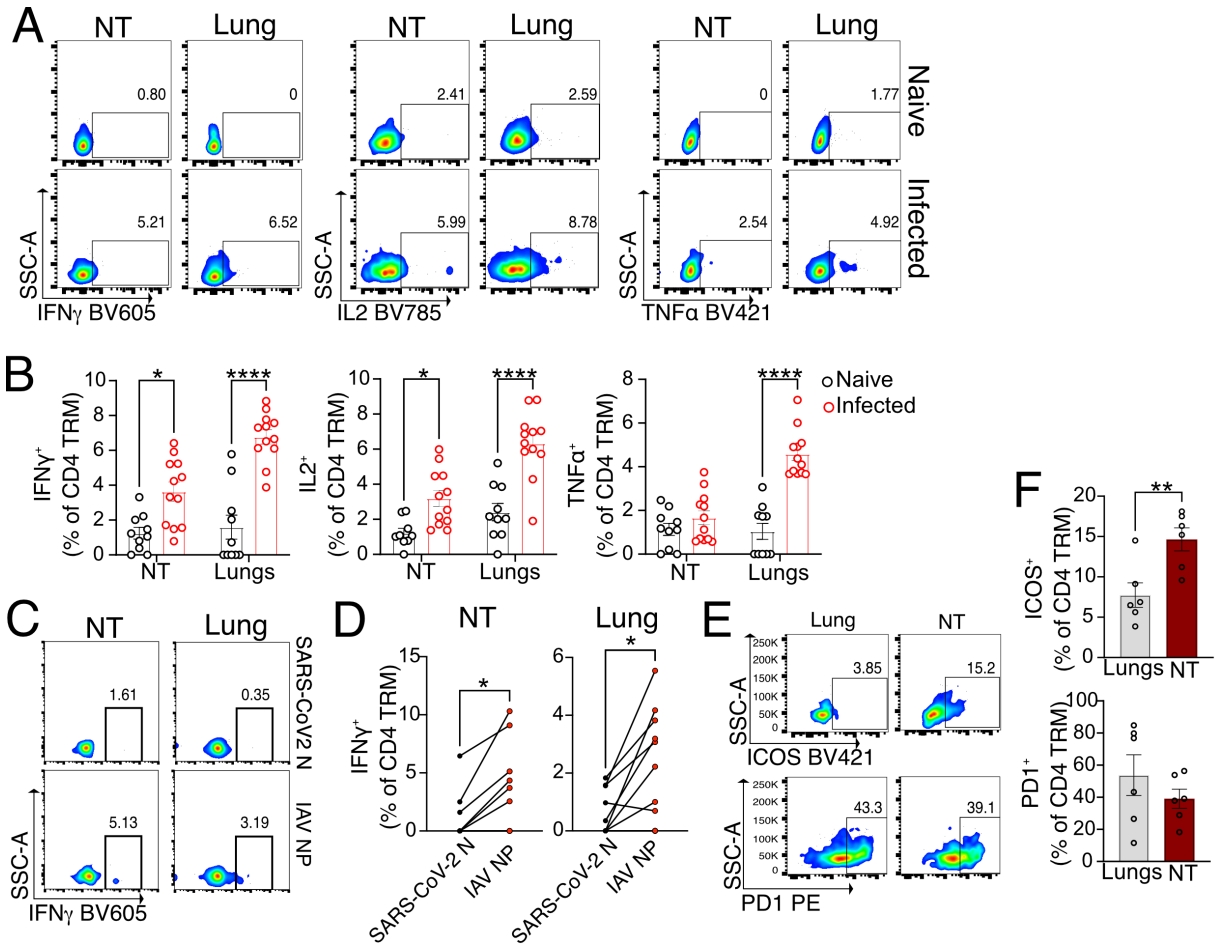

Fig 2: NT CD4 TRM express cytokines upon antigen stimulation

A-B) Expression of intracellular cytokines in CD4 TRM of NT and lungs upon restimulation with IAV NP peptide pool. The organs are isolated on day 30 following PR8 IAV infection of mice or from naïve mice. A) Flow cytometry plots indicating the percentage of CD4 TRM expressing IFN-γ, IL-2 and TNF. B) Scatter plot showing the percentage of CD4 TRM expressing IFN-γ, IL-2 and TNF. The experiment was repeated thrice and the results (mean ± s.e.m.) are pooled. NS, not significant, ****P<0.0001; ***P<0.001; **P<0.01; *P<0.05 by two-way ANOVA, with Tukey's multiple comparison test.

C-D) Frequency of IFNγ$^+$ cells among all lung and NT CD4 TRM isolated on day 30 post PR8 infection and that are stimulated with peptide pool (IAV NP versus SARS-CoV-2 nucleocapsid) pulsed splenocytes. C) Representative flow cytometry plots showing the expression of IFNγ$^+$ cells among all lung and NT CD4 TRM. D) Graph indicating the IFNγ$^+$ cells among CD4 TRM stimulated by IAV NP versus SARS-CoV-2 nucleocapsid pulsed splenocytes connected by a line. Each line indicates an individual mouse. The experiment was performed three times and the results were pooled. NS, not significant, ****P<0.0001; ***P<0.001; **P<0.01; *P<0.05 by two-sided Wilcoxon matched-pairs signed-rank test.

E-F) Expression of ICOS and PD-1 on CD4 TRM on d30 post PR8 IAV infection. E) Representative flow cytometry plots of CD4 TRM expressing ICOS and PD-1 in lungs and NT. F) Scatter plot showing the percentage of CD4 TRM expressing ICOS and PD-

1412 1. The experiment was repeated twice and the results (mean ± s.e.m.) are pooled. NS,
1413 not significant, ****P<0.0001; ***P<0.001; **P<0.01; *P<0.05 by unpaired two-tailed
1414 t-test.
1415

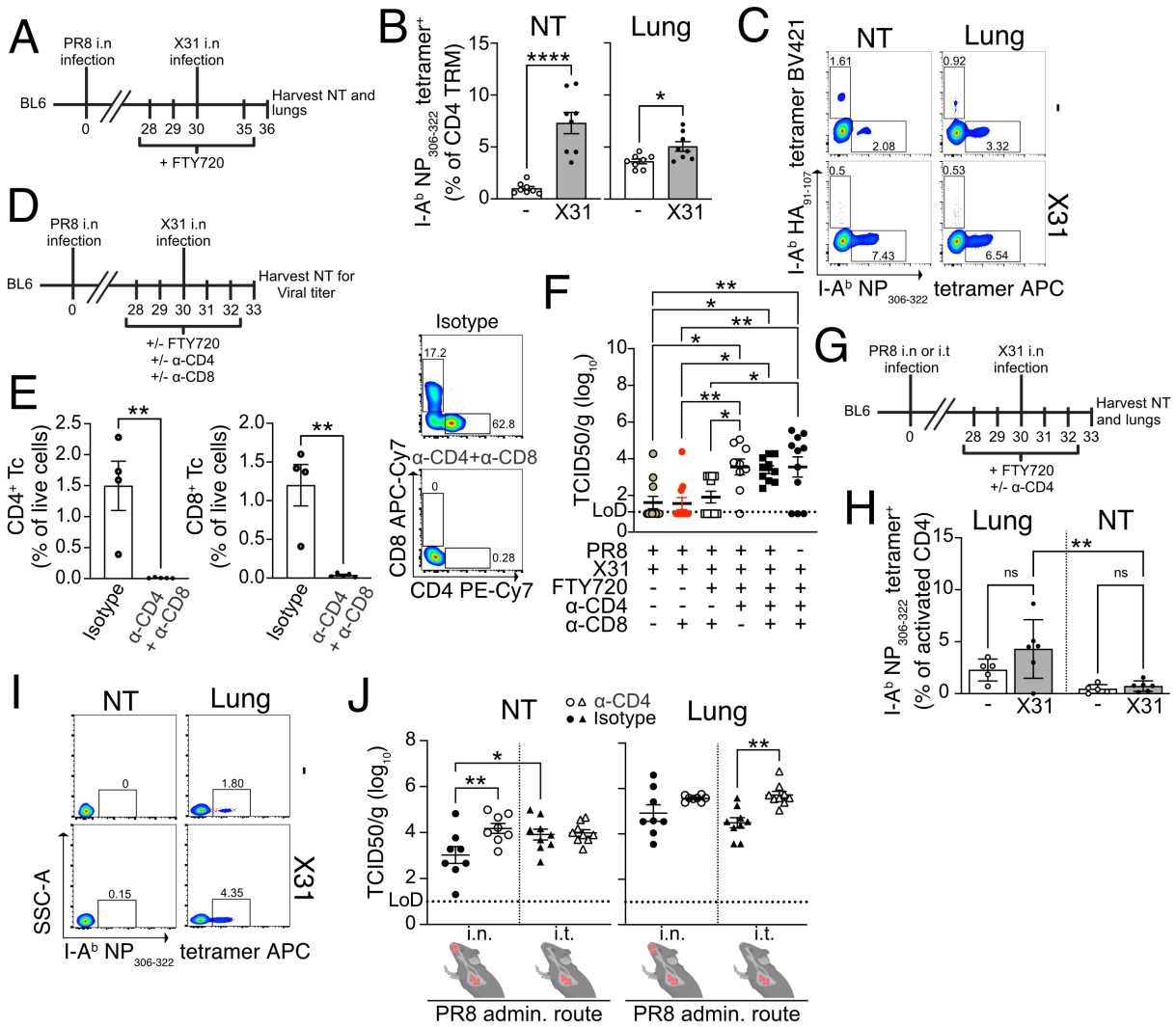

Fig 3: NT CD4 TRM provide protection against heterosubtypic challenge

A-C) I-A^b NP$_{306-322}$ tetramer and I-A^b HA$_{91-107}$ tetramer-specific CD4 TRM in the NT and lungs of mice that were infected with X31 intranasally or left uninfected on day 30 following PR8 infection. The mice were treated with FTY720 and the organs were analyzed 6 days post X31 infection. A) Schematic representation of the experimental setup. B) Scatter plot indicating the percentage of I-A^b NP$_{306-322}$ tetramer$^+$ cells among CD4 TRM of lungs and NT. The experiment was done twice and the results (mean ± s.e.m.) were pooled. NS, not significant, ****P<0.0001; ***P<0.001; **P<0.01; *P<0.05 by unpaired two-tailed t-test. C) Representative flow cytometry plots indicating the percentages of I-A^b NP$_{306-322}$ tetramer and I-A^b HA$_{91-107}$ tetramer- specific CD4 TRM are shown.

D) Schematic representation of primary and secondary infection of mice, their treatment with anti-CD4 antibody, anti-CD8 antibody or/and FTY720 on the indicated days and collection of NT.

E) Left panel: Scatter plot showing the frequency of CD4 Tc and CD8 Tc among all live cells in the NT of mice treated with isotype control antibody or anti-CD4 and anti-CD8 antibody. The experiment was performed once. The result is shown as (mean ± s.e.m.)

1434 NS, not significant, ****P<0.0001; ***P<0.001; **P<0.01; *P<0.05 by unpaired two-
1435 tailed t-test. Right panel: A representative flow cytometry plot for the frequency of CD4
1436 and CD8 Tc.
1437 F) Scatter plot indicating viral titers ($TCID_{50}$/g) in NT of mice on day 3 following
1438 secondary infection with X31 IAV. The experiment was repeated thrice and the results
1439 (mean ± s.e.m.) are pooled. NS, not significant, ****P<0.0001; ***P<0.001; **P<0.01;
1440 *P<0.05 by one-way ANOVA, with Dunnet multiple comparison test. The outliers were
1441 identified and removed using Grubbs method (alpha=0.05). One outlier each removed
1442 from all groups except for groups: PR8 + anti-CD8 + FTY720 and PR8 + anti-CD4.

1443 G-J) Viral titer and frequency of I-A^b $NP_{306-322}^+$ CD4 TRM in the NT and lungs of mice who
1444 have undergone intratracheal or intranasal PR8 infection followed by intranasal
1445 infection with X31 on day 30 post primary infection. The mice were treated with
1446 FTY720+/- anti-CD4 antibody or left untreated. G) Schematic representation of the
1447 experimental set up. H) Scatter plot indicating the frequency of I-A^b $NP_{306-322}$
1448 tetramer$^+$CD4iv$^-$CD44$^+$CD62L$^-$ cells in the NT and lungs of mice on day 3 post-
1449 secondary X31 infection +FTY720 treatment vs mice without secondary X31 infection
1450 and not treated with FTY720 as shown in fig 3G. The experiment was repeated thrice
1451 and the results (mean ± s.e.m.) are pooled. NS, not significant, ****P<0.0001;
1452 ***P<0.001; **P<0.01; *P<0.05 by two-way ANOVA, with Tukey's multiple
1453 comparison test. I) Representative flow cytometry plots indicating percentages of I-A^b
1454 $NP_{306-322}$ tetramer$^+$CD4iv$^-$CD44$^+$CD62L$^-$ cells in NT and lung of mice with and without
1455 secondary X31 infection (related to 3H). J) Scatter plot showing viral titers ($TCID_{50}$/g)
1456 in NT and lungs of mice on day 3 following secondary infection with X31 IAV and who
1457 were infected with PR8 intranasally or intratracheally 30 days prior to X31 infection.
1458 The mice were treated with FTY720 ip as indicated in fig 3G. The experiment was
1459 repeated twice and the results (mean ± s.e.m.) are pooled. NS, not significant,
1460 ****P<0.0001; ***P<0.001; **P<0.01; *P<0.05 by one-way ANOVA, with Dunnet
1461 multiple comparison test.
1462
1463
1464

1465

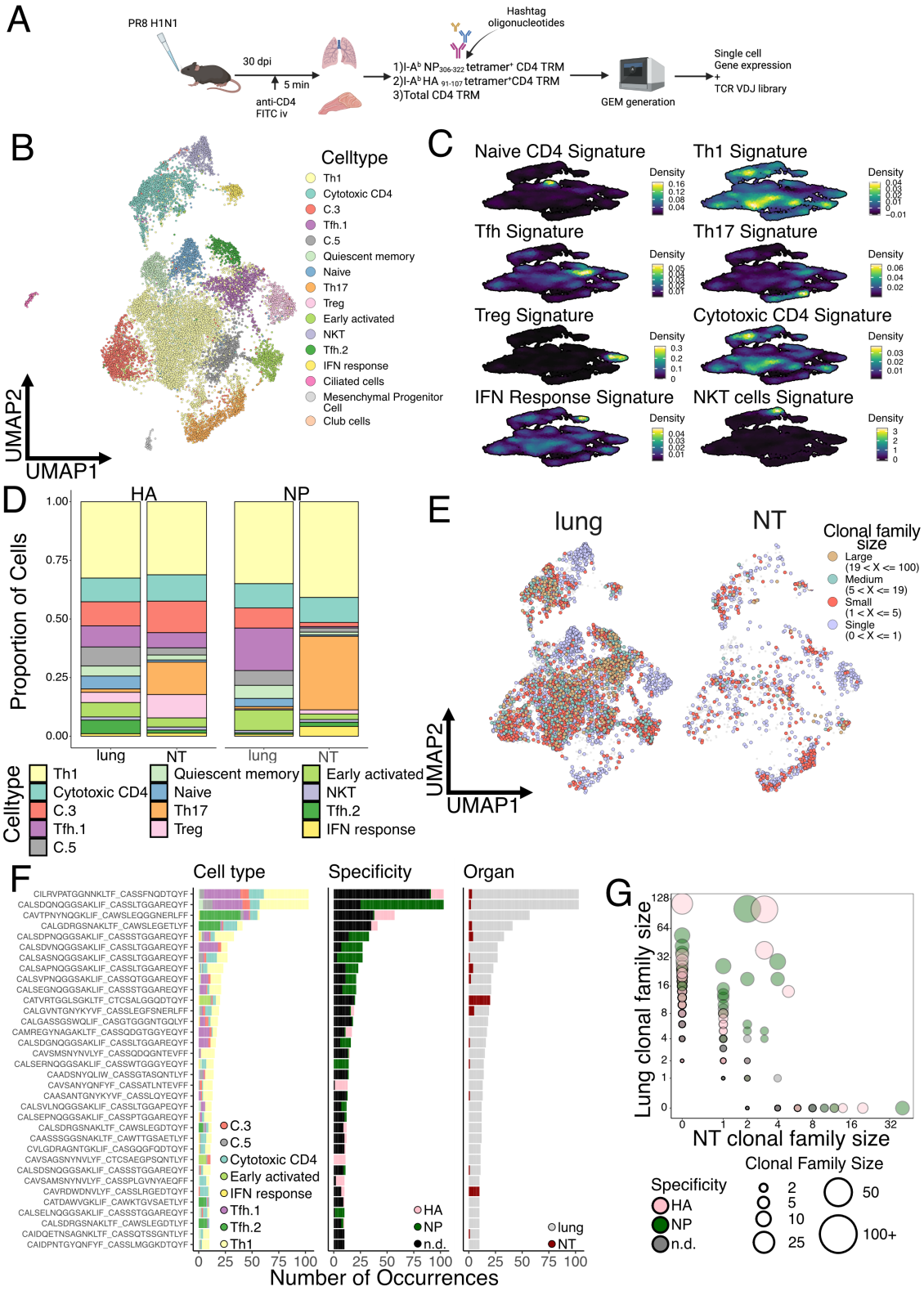

Fig 4: Single cell RNA and TCR sequencing of CD4 TRM reveals differential cluster distribution but clonal sharing between organs

1470
1471 A) Schematic diagram showing the preparation of antigen-specific cells from PR8 IAV
1472 infected mice for generation of GEM using 10X Chromium controller.
1473 B) UMAP plot of unsupervised clustering for 15301 CD4 TRM isolated from lungs and NT
1474 of naïve and PR8 IAV infected mice.
1475 C) Density plot showing the expression of selected gene signatures, projected on the same
1476 UMAP as in B. Naïve CD4 T signature(Wang et al., 2022), Th1 signature(Andreatta et
1477 al., 2022), Tfh signature(Andreatta et al., 2022), Th17 signature(Szabo et al., 2019a),
1478 Treg signature(Yang et al., 2021), Cytotoxic CD4 signature(Hashimoto et al., 2019),
1479 IFN response signature(Szabo et al., 2019a), NKT cells signature(Cohen et al., 2013; Hu
1480 et al., 2022).
1481 D) Bar graph showing proportion of each UMAP cluster divided by organ and antigen
1482 specificity. Only antigen specific CD4 TRM from infected mice were included in the
1483 analysis.
1484 E) UMAP plot split by tissue (lung or NT) and colored according to clone size for CD4
1485 TRM in IAV infected mice. Clones were binned into single clones (1 member; light
1486 blue), small (2 to 5 members; red), medium (6 to 19 members; green), large (over 20
1487 members; gold). Light grey dots represent cells where TCR clonotype could not be
1488 assigned.
1489 F) Bar plot characterizing the top 34 most expanded clones. The y axis reports CDR3
1490 sequences of TCRαβ while the bar graphs show the number of cells divided according
1491 to cluster distribution, I-A^b $NP_{306-322}$ tetramer$^+$ or I-A^b HA_{91-107} tetramer$^+$ and organ
1492 specificity. n.d. = not determined.
1493 G) Graph showing clonal relationship between lungs and NT from PR8 IAV infected mice.
1494 Each circle indicates one clonal family and size of the circle defines the size of the clonal
1495 family. Color of the circle denotes the antigenic specificity against I-A^b $NP_{306-322}$
1496 tetramer and against I-A^b HA_{91-107} tetramer. n.d. = not determined.
1497

1498

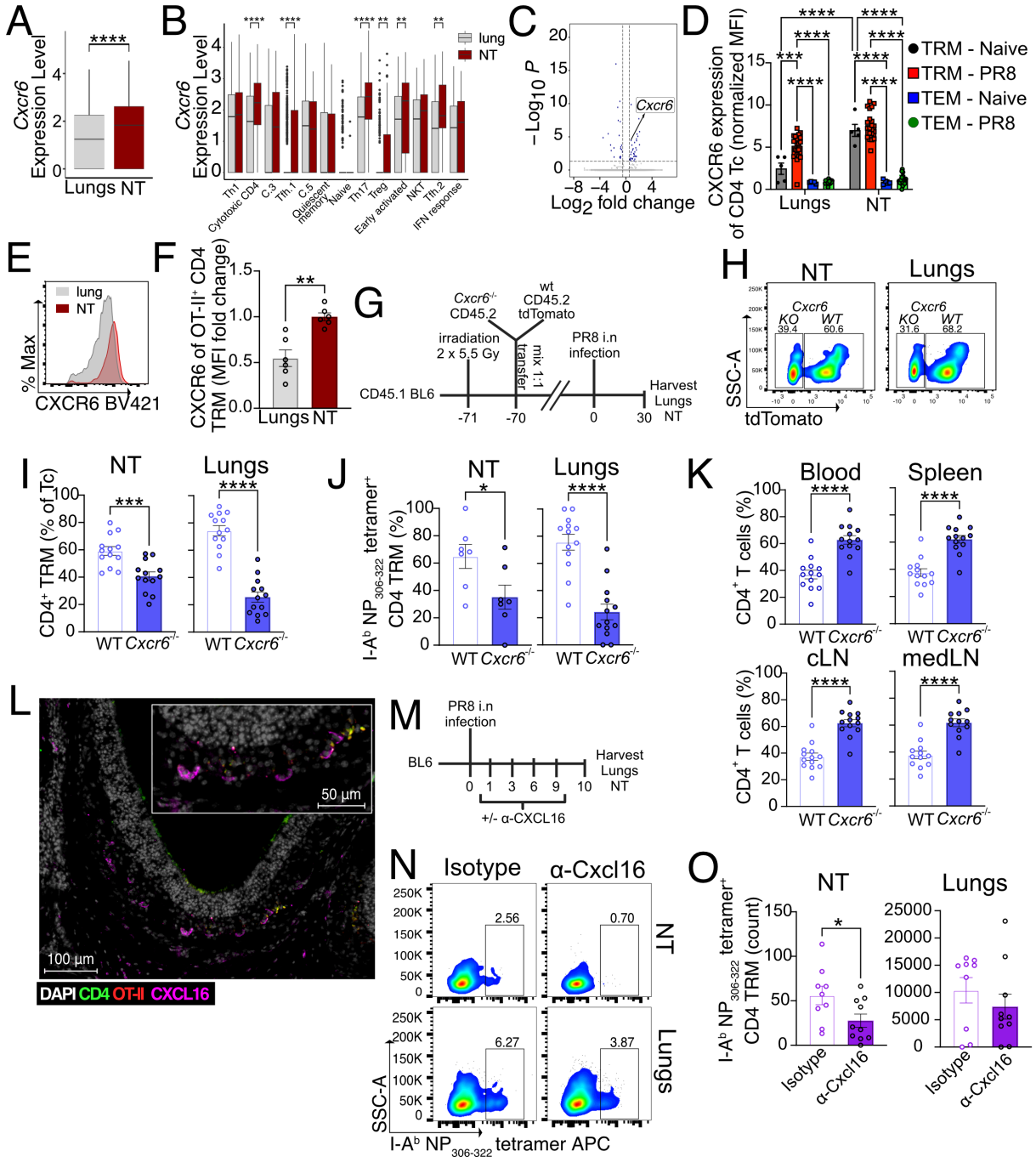

Fig 5: CXCR6-CXCL16 axis promotes NT CD4 TRM establishment

A) Box plot showing the expression of *Cxcr6* mRNA among CD4 TRM of the NT and lungs. Data are presented as median and interquartile range. NS, not significant, ****$P<0.0001$; ***$P<0.001$; **$P<0.01$; *$P<0.05$ by unpaired two-tailed t-test.

B) Box plot showing the expression of *Cxcr6* mRNA among different cell clusters of lungs and NT. Data are presented as median and interquartile range. NS, not significant, ****$P<0.0001$; ***$P<0.001$; **$P<0.01$; *$P<0.05$ by Wilcoxon rank sum test with Benjamini-Hochberg correction

1509 C) Volcano plot for differential expressed genes in the NT in comparison to the lungs of
1510 the Th17 cluster. The dotted lines indicate fold change and adjusted p value cutoffs.
1511 D) Bar plot for the expression of CXCR6 (each Median Fluorescence Intensity (MFI)
1512 normalized to mean MFI from CD4 TEM iv^+ of NT) in CD4 TRM and iv^+ CD4 TEM
1513 from the lungs and NT of naïve mice and PR8 IAV infected mice (30 dpi) as indicated.
1514 The experiment was repeated thrice and the results (mean ± s.e.m.) are pooled. NS, not
1515 significant, ****P<0.0001; ***P<0.001; **P<0.01; *P<0.05 by two-way ANOVA,
1516 with Tukey's multiple comparison test.

1517 E-F) Expression of CXCR6 on OT-II CD4 TRM of NT and lung on d30 following PR8-OVA
1518 infection as indicated. E) Representative histograms for CXCR6 expression from OT-II
1519 CD4 TRM of NT and lung are shown. F) Scatter plot showing the expression of CXCR6
1520 (each Median Fluorescence Intensity (MFI) normalized to mean MFI of NT OT-II CD4
1521 TRM). The experiment was repeated thrice and the results (mean ± s.e.m.) are pooled.
1522 NS, not significant, ****P<0.0001; ***P<0.001; **P<0.01; *P<0.05 by unpaired two-
1523 tailed t-test.
1524 G-K) Frequency of different cell populations within different organs derived from WT- *Cxcr6*-
1525 /- BM chimeric mice on day 30 post infection with PR8 IAV as indicated. G) Schematic
1526 representation of the experimental setup. H) Representative flow cytometry plots
1527 showing the percentage of WT and *Cxcr6*$^{-/-}$ CD4 TRM in NT and lungs. I) Scatter plot
1528 for the percentage of WT and *Cxcr6*$^{-/-}$ CD4 TRM in NT and lungs as indicated. J) Scatter
1529 plot for the percentage of I-A^b $NP_{306-322}$ tetramer - specific WT and *Cxcr6*$^{-/-}$ CD4 TRM
1530 in NT and lungs as indicated. Samples that had less than 7 OT-II CD4 TRM were
1531 excluded from the analysis. The experiment was repeated thrice and the results (mean
1532 ± s.e.m.) are pooled. NS, not significant, ****P<0.0001; ***P<0.001; **P<0.01;
1533 *P<0.05 by unpaired two-tailed t-test. K) Scatter plot showing the percentage of *Cxcr6*-
1534 /- and WT CD4 T cells in different organs of the BM chimera on day 30 post infection
1535 with PR8. The experiment was repeated thrice and the results (mean ± s.e.m.) were
1536 pooled. NS, not significant, ****P<0.0001; ***P<0.001; **P<0.01; *P<0.05 by
1537 unpaired two-tailed t-test.
1538 L) A representative microscopic image of CXCL16 expression (magenta) and OT-II CD4
1539 T cells (red and green) in the olfactory epithelium of the murine NT. NT is isolated on
1540 day 30 post PR8-OVA infection from mice that received OT-II CD4 T cells.
1541 M-O) Antigen-specific CD4 TRM in the lungs and NT of mice treated with isotype control or
1542 anti-CXCL16 antibody on day 10 post PR8 IAV infection. M) Schematic representation
1543 of the experimental setup. N) Representative flow cytometry plots indicating the
1544 percentage of I-A^b $NP_{306-322}$ tetramer - specific CD4 TRM are shown. O) Scatter plot
1545 indicating the absolute number of I-A^b $NP_{306-322}$ tetramer - specific CD4 TRM. The
1546 experiment was performed twice and the results (mean ± s.e.m.) are pooled. NS, not
1547 significant, ****P<0.0001; ***P<0.001; **P<0.01; *P<0.05 by unpaired two-tailed t-
1548 test.
1549

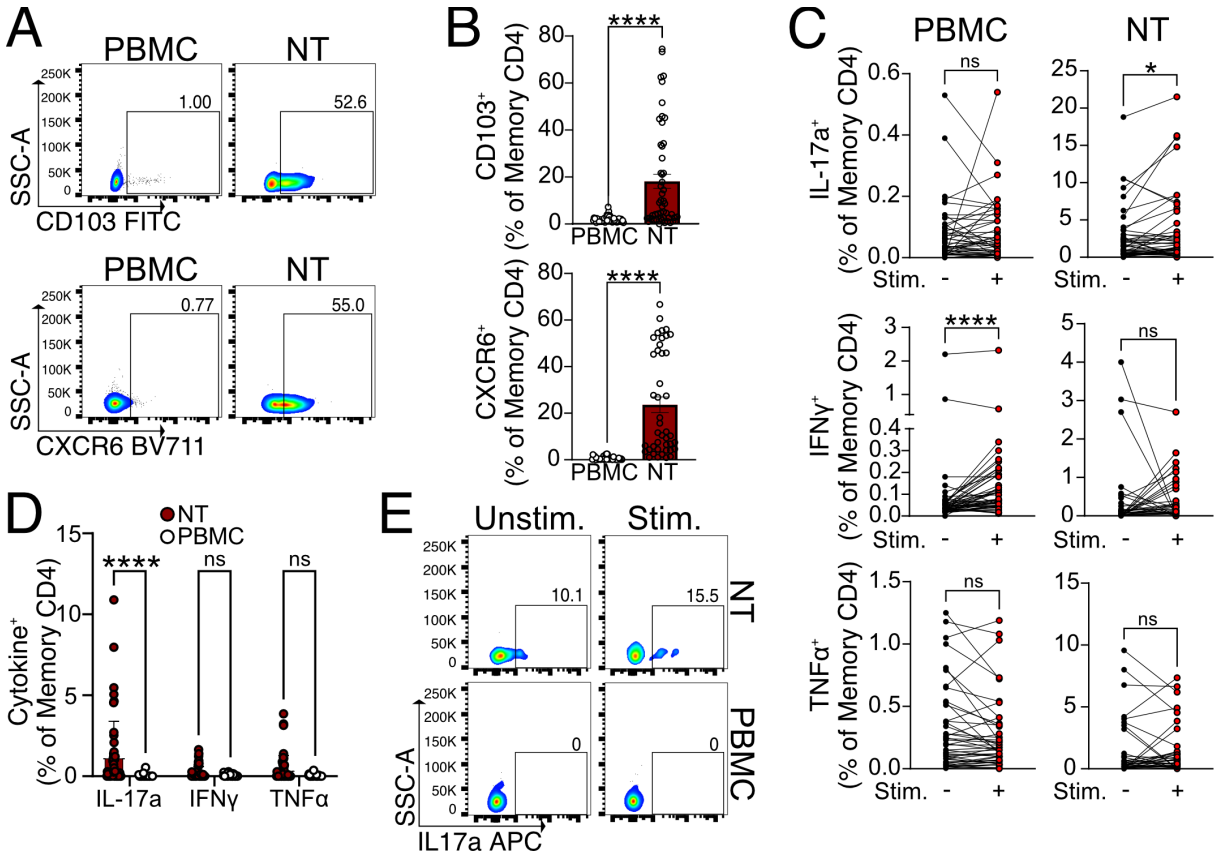

Fig 6: Functional IAV-specific CD4 TRM exist in the nasopharynx of healthy human subjects

A-B) Expression of CD103 and CXCR6 on NT CD4 TRM and CD4 TEM of PBMC derived from healthy human subjects. A) Representative flow cytometry plots indicating the percentage of CD103 and CXCR6 expression on CD4 TRM and CD4 TEM from the same subject. B) Scatter plot showing the percentage of CD103 and CXCR6 expression on CD4 TRM and CD4 TEM. Each data point indicates one subject. The experiment was performed five times and the results (mean ± s.e.m.) are pooled. NS, not significant, ****P<0.0001; ***P<0.001; **P<0.01; *P<0.05 by unpaired two-tailed t-test.

C) Percentage of NT CD4 TRM and CD4 TEM from PBMC expressing IL-17a, IFN-γ and TNFα. The cytokine expression is indicated from unstimulated cells and IAV NP peptide pool and M1 peptide pool stimulated cells connected by a line. Each line on the graph indicates cytokine expression from the cells of each subject. NS, not significant, ****P<0.0001; ***P<0.001; **P<0.01; *P<0.05 by two-sided Wilcoxon matched-pairs signed-rank test.

D) Scatter plot showing the percentage of NT CD4 TRM and CD4 TEM from PBMC expressing IL-17a, IFN-γ and TNF after stimulation with IAV NP peptide pool and M1 peptide pool (after subtraction of signals from the unstimulated control; negative values considered zero). The experiment was performed seven times and the results (mean ± s.e.m.) are pooled. NS, not significant, ****P<0.0001; ***P<0.001; **P<0.01; *P<0.05 by two-way ANOVA, with Tukey's multiple comparison test.

1572 E) Representative flow cytometry plots showing the expression of IL-17a in NT CD4 TRM
1573 and CD4 TEM of PBMC which are stimulated with IAV NP peptide pool and M1
1574 peptide pool or left unstimulated.

1575

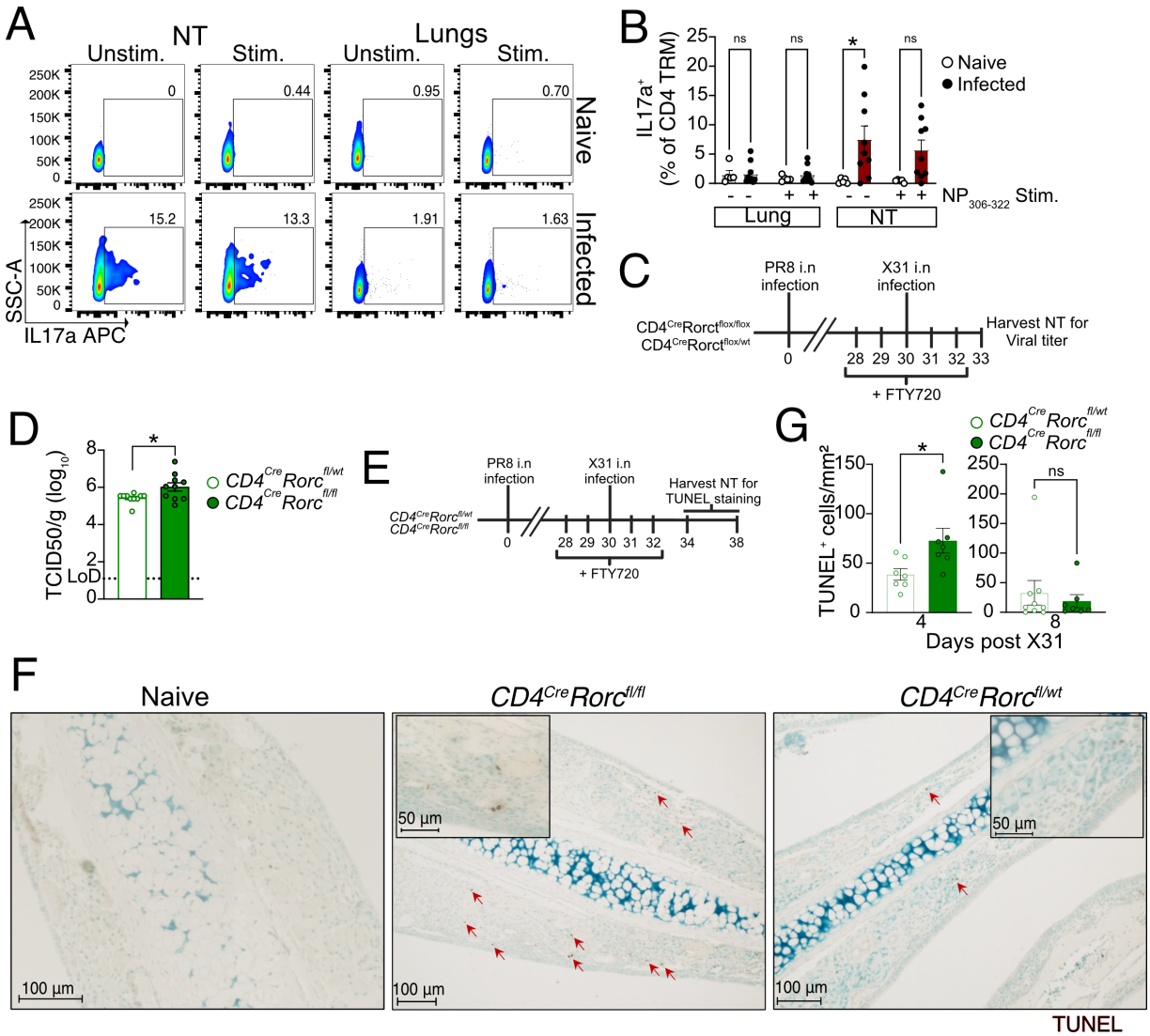

Fig 7: NT harbors Th17 CD4 TRM that reduce local pathology

A-B) Frequency of IL-17a$^+$ cells among CD4 TRM of NT and lungs upon restimulation with IAV immunodominant $NP_{306-322}$ peptide in comparison to unstimulated cells. The organs are isolated on day 30 following PR8 IAV infection of mice and from naïve mice. A) A representative flow cytometry plot showing the percentage of IL-17a in lungs and NT. B) Scatter plot indicating the frequency of IL-17a$^+$ cells among all CD4 TRM. The experiment was repeated twice and the results (mean ± s.e.m.) are pooled. NS, not significant, ****P<0.0001; ***P<0.001; **P<0.01; *P<0.05 by two-way ANOVA, with Tukey's multiple comparison test.

C-D) Viral titers in the NT of *CD4^{cre}Rorct$^{fl/fl}$* and *CD4^{cre}Rorc$^{fl/wt}$* mice on day 3 following secondary infection with X31 IAV. The mice were infected with PR8 and reinfected with X31 IAV on day 30 post primary infection and treated with fingolimod ip as indicated. C) A schematic representation of the experimental setup. D) Scatter plot showing viral titers ($TCID_{50}$/g) in the NT of the two groups. The experiment was

1593 repeated twice and the results (mean ± s.e.m.) are pooled. NS, not significant,
1594 ****P<0.0001; ***P<0.001; **P<0.01; *P<0.05 by unpaired two-tailed t-test.
1595 E-G) Microscopy for TUNEL^{+} cells in the nasal septum (respiratory region) derived from
1596 *CD4^{cre}Rorc$t^{fl/fl}$* and *CD4^{cre}Rorc$^{fl/wt}$* mice. The mice were infected with PR8 and
1597 reinfected with X31 IAV on day 30 following PR8 IAV infection. The tissues were
1598 isolated on day 4 and day 8 following X31 IAV infection. E) A schematic representation
1599 of the experimental setup. F) Representative microscopic images for TUNEL^{+} cells
1600 (brown) in the nasal septum from mice on day 4 post X31 IAV infection are shown.
1601 Scale bar: 100µm. G) Scatter plot showing the number of TUNEL^{+} cells per mm2 in the
1602 respiratory region of the nasal septum. The experiment was repeated twice and the
1603 results (mean ± s.e.m.) are pooled. NS, not significant, ****P<0.0001; ***P<0.001;
1604 **P<0.01; *P<0.05 by two-way ANOVA, with Tukey's multiple comparison test.
1605
1606